

The Modelling of Feedback Processes in Cosmological Simulations of Disk Galaxy Formation

Franziska Piontek and Matthias Steinmetz
Astrophysikalisches Institut Potsdam, An der Sternwarte 16, 14482 Potsdam, Germany

ABSTRACT

We present a systematic study of stellar feedback processes in simulations of disk galaxy formation. Using a dark matter halo with properties similar to the ones for the Milky Way’s stellar halo, we perform a comparison of different methods of distributing energy related to feedback processes to the surrounding gas. A most promising standard model is applied to halos spanning a range of masses in order to compare the results to disk galaxy scaling relations. With few exceptions we find little or no angular momentum deficiency for our galaxies and a good agreement with the angular momentum-size relation. Our galaxies are in good agreement with the baryonic Tully-Fisher relation and the slope of the photometric Tully-Fisher relation is reproduced. We find a zero-point offset of 0.7 to 1 magnitudes, depending on the employed IMF. We also study our standard feedback model in combination with additional physical processes like a UV background, kinetic feedback, a delayed energy deposition as expected for type Ia supernovae, mass return and metal-dependent cooling. Only a combination of effects yields a real improvement of the resulting galaxy by reducing the bulge, while including metal-dependent cooling increases the bulge again. We find that in general the stellar mass fraction of our galaxies is too high. In an ad-hoc experiment we show that an removal of the bulge could reconcile this. However, the fit of the Tully-Fisher relation can only be improved by delaying the star formation, but not suppressing it completely. Our models do not seem to be efficient enough to achieve either effect. We conclude that disk formation is a complex, highly interconnected problem and we expect a solution to come from a combination of small effects.

Key words: galaxies: spiral - formation - evolution - structure - methods: N -body simulations - hydrodynamics

1 INTRODUCTION

The formation of galaxies is a complex process governed by gravitational collapse and an energetic coupling between the interstellar (and also intergalactic) gas and stellar evolution processes. This includes the cooling of gas and subsequent formation of stars as well as loss of mass and energy through stellar winds and supernova explosions which is known as stellar feedback. Such feedback is essential for the success of the widely accepted hierarchical model of galaxy formation (White & Rees 1978). It regulates star formation by particularly preventing stars from forming too early which would lead mostly to galaxies dominated by large, old spheroids instead of disks (White & Frenk 1991). This is inconsistent with observations showing that up to 70% of $\sim 10^{12} h^{-1} M_{\odot}$ halos host disk dominated late-type galaxies in the present day universe (e.g. Weinmann et al. 2006; Park et al. 2007). Feedback affects the thermodynamics of the interstellar medium (ISM) in two ways. In supernova explosions, large amounts of energy heat the surrounding

gas and disrupt cold clouds, therefore efficiently quenching star formation. At the same time, the surrounding gas is enriched with metals produced in stars enabling more efficient cooling (Sutherland & Dopita 1993) and therefore increasing star formation. All of these processes happen on scales of a few to tens of parsecs which is well below current achievable resolution of cosmological simulations (see however Ceverino & Klypin 2009). Therefore a range of so called “subgrid models” have been developed to model at least the effects on larger, galactic scales (for example Okamoto et al. (2005), Scannapieco et al. (2006), Springel & Hernquist (2003), Stinson et al. (2006)). Compared to early work (for example Steinmetz & Müller 1995; Navarro & Steinmetz 1997) and in combination with improved resolution, this has recently led to considerable improvement in reproducing individual realistic disk galaxies (see Abadi et al. (2003a), Governato et al. (2004), Governato et al. (2007), Okamoto et al. (2005), Robertson et al. (2004), Scannapieco et al. (2008)), though still none of them fulfilled all characteristics of typical ob-

served late-type spirals. Furthermore, none of them resembled a bulge-less disk galaxy, despite of their non-negligible numbers in the local universe (Kautsch et al. 2006). The fundamental question of disk galaxy formation therefore is still open.

All successful attempts to model disk galaxies which have been achieved so far were simulated using handpicked dark matter halos and carefully calibrated codes. Recent work by Scannapieco et al. (2009) demonstrated that, when applying their model to a random sample of halos, only a small fraction had a disk component and none was disk dominated. Furthermore, Scannapieco et al. (2009) questions the usual assumption that Hubble type and formation history are directly correlated. Considering the large abundances of disk galaxies, this indicates that we may still lack an understanding of the big picture. Furthermore, disks are susceptible to mergers which are more common at high redshift and typically result in the formation of a spheroid (Peebles 1982; Blumenthal et al. 1984; Davis et al. 1985; Gottlöber et al. 2001; Wechsler et al. 2002; Cole et al. 2008; Wetzel et al. 2009). One possible way out is to re-grow a disk after a major merger, provided the merging progenitor disks are gas-rich (Robertson et al. 2006; Bullock et al. 2009). A first example of this in a cosmological simulation has been presented recently by Governato et al. (2008), but again it is an isolated case.

The work we present in this paper focuses on furthering the understanding of the physical requirements of disk formation. The main question addressed by our feedback study can be phrased as follows: Which of the many ingredients of the range of models summarized above are necessary, which are sufficient and how exactly do they influence the galaxy formation process alone and in combination? As in our study of the angular momentum problem (Piontek & Steinmetz 2009, Paper 1 hereafter), we follow our strategy of slowly increasing the complexity of the model. First using a pre-selected dark matter halo with a mass similar to the halo of the Milky Way, with a high spin parameter and a quiet merging history, usually thought to be the most likely to host a disk, we study different methods of distributing feedback energy. The best result becomes our standard model, which we then apply to a set of halos with a range of different masses and a second set of Milky Way-type halos but with different merging histories. We also study a set of simulations examining other relevant physical effects. We carefully analyze the resulting disk to understand the influence each of these effects has alone, before we put several physical effects together for our most realistic model of galaxy formation.

The paper is organized as follows. In §2 we describe the initial conditions, the code and the analysis methods we use. The study of feedback energy distribution methods is covered in §3. §4 contains the study of halos with different assembly histories, §5 the study of halos with different masses and §6 the application of additional physics besides the standard feedback model. A detailed description of our most complex model can be found in §7 and the influence of the additional physics on the scaling relations is discussed in §8. We discuss our findings and conclude in §9.

2 INITIAL CONDITIONS, CODE AND ANALYSIS METHODS

2.1 Code

The simulations are done with the N-body code GADGET2 (Springel 2005) using the Smoothed Particle Hydrodynamics (SPH) framework (Gingold & Monaghan (1977), Lucy (1977)) for the gas and an implementation of radiative cooling courtesy of Volker Springel and based on Katz et al. (1996). For simplicity, in the standard cases we do not include an external UV background. Star formation is implemented following Katz (1992) and is already described in detail in Paper 1. It is motivated by a Schmidt law (Schmidt 1959) giving the star formation rate as

$$\frac{d\rho_\star}{dt} = c_\star \frac{\rho_{gas}}{t_\star} \quad (1)$$

with $c_\star=0.1$ and $t_\star=\max(t_{dyn},t_{cool})$, and then the application of a stochastic approach. We assume that each gas particles can spawn two generations of stars, so each star particle has half the mass of a gas particle. Necessary conditions for star formation are a critical density of $\rho_{crit}=7\times 10^{-26}\text{g cm}^{-3}$, a converging flow and a low temperature of $T < 3\times 10^4$ K.

2.2 Initial conditions

All of our halos are resimulations (see Navarro & White 1994) from a large cosmological box with $64\text{ h}^{-1}\text{ Mpc}^3$ box size. We use the WMAP3 cosmology (Spergel et al. 2007) with $H_0=73\text{ km s}^{-1}\text{ Mpc}^{-1}$, $\sigma_8=0.75$, $n_{rms}=0.9$, $\Omega_0=0.24$ and $\Omega_\Lambda=0.76$. The simulations start at $z=50$. Gas particles are added on top of each dark matter particle assuming the cosmological baryon density, $\Omega_{bar}=0.04$. Our standard halo (MW_mr) is a halo with a mass similar to the Milky Way (about $10^{12}\text{ h}^{-1}\text{ M}_\odot$ Smith et al. 2007; Xue et al. 2008), with a fairly quiet merging history and a comparatively high spin parameter $\lambda=0.054$. Our standard resolution corresponds to 1024^3 effective particles within the high resolution region surrounding our target halo. This translates to particle masses of $2.8\times 10^6\text{ h}^{-1}\text{ M}_\odot$ for gas and $1.34\times 10^7\text{ h}^{-1}\text{ M}_\odot$ for dark matter particles, and we use a softening of 1.5 and $2\text{ h}^{-1}\text{ kpc}$ respectively. Additionally, we selected three halos comparable in mass to the standard halo, but with very different merging histories, to study the influence of the merging history of the host halo on the formation of the disk. Lastly, we selected six halos with smaller masses starting at $\approx 10^{11}\text{ M}_\odot$ and one halo with a larger mass of $\approx 2\times 10^{12}\text{ M}_\odot$ to sample the disk galaxy scaling relations over a larger mass range. All halos were selected to have no object of equal or larger mass close by. All the lower mass halos and also the standard halo have been simulated in high resolution with 2048^3 effective particles in the resimulation region and particle masses and gravitational softening parameters of $3.54\times 10^5\text{ h}^{-1}\text{ M}_\odot$, $1.7\times 10^6\text{ h}^{-1}\text{ M}_\odot$ and 0.75 and $1\text{ h}^{-1}\text{ kpc}$, respectively. Table 1 shows an overview of characteristic parameters of the halos we simulate.

2.3 Analysis

We define our halos using R_{vir} via $\rho(R_{vir}) = \Delta\rho_c$ with $\rho_c = 3H_0^2/(8\pi G)$ and $\Delta = 18\pi^2 + 82x - 39x^2$, $x =$

halo	M_{vir} $10^{12} M_{\odot}$	R_{vir} kpc	V_{vir} km s^{-1}	λ	z_{lmm} (1:3)	effective resolution	N_{vir}
MW_mr	1.26	296	146.17	0.054	3.63	1024^3	1.6×10^5
MW_hr	1.23	290	143.22	0.058	3.63	2048^3	10^6
MW_mh1_mr	1.24	294	145.66	0.023	4.85	1024^3	1.55×10^5
MW_mh2_mr	1.23	298	137.2	0.063	1.18	1024^3	1.8×10^5
MW_mh3_mr	1.2	291	144.2	0.05	1.35	1024^3	1.5×10^5
DM_hr1	0.135	139	68.32	0.04	4.56	2048^3	10^5
DM_hr2	0.252	173	85.11	0.029	3.02	2048^3	2.42×10^5
DM_hr3	0.358	193	95.34	0.034	3.44	2048^3	3.13×10^5
DM_hr4	0.493	214	105.5	0.019	6.09	2048^3	4.2×10^5
DM_hr5	0.594	227	112.38	0.016	3.44	2048^3	5×10^5
DM_hr6	0.703	241	119.36	0.026	3.83	2048^3	6.1×10^5
DM_mr7	2.36	364	180.37	0.018	4.556	1024^3	2.85×10^5

Table 1. Characteristic parameters for our halos run with the standard feedback model. MW labels our standard, Milky Way-type halo, MW_mh halos with the same mass but varying merging histories (mh) and DM_hr1 to 7 halos with different masses. lr, mr and hr indicate the effective resolution of the high resolution region shown in the second to last column. N_{vir} is the approximate total number of gas, star and dark matter particles in R_{vir} in the runs with the standard feedback model. This slightly varies for different feedback models, but the order of magnitude stays the same.

$\Omega_0(1+z)^3/(\Omega_0(1+z)^3 + \Omega_{\Lambda}) - 1$. Characteristic parameters for the galaxy are calculated using all particles within a sphere of $6R_{\text{d}}$. For the Milky Way with $R_{\text{d}} \approx 3.5$ kpc, this corresponds to the disk radius. For our simulated galaxies with larger scale lengths, $6R_{\text{d}}$ corresponds approximately to the size of the Milky Way stellar halo Schneider (2006). R_{d} is the disk scaling length. As gaseous disk we define the cold gas (with $T < 3 \times 10^4 \text{K}$) in the center of the halo, which forms a clearly distinguishable disk. In most cases, there is only little hot gas surrounding the cold disk. We rotate the galaxy so that the disk is in the x-y plane. Rotational velocities are measured at $2.2R_{\text{d}}$ using the rotation curve of the disk gas. This is close to observational measures of rotational velocities which are often obtained using HI observations (for example de Blok et al. 2008). An example for rotation curves with the standard halo and standard feedback model is shown in Figure 1 for the standard and the high resolution run. Our rotation curves are fairly flat, though particularly in the smaller halos, and in the more bulge dominated models, they can be steeper than shown here. However, the difference between the measured rotational velocity at the peak and at the adopted radius, even for our steeper curves, is never more than 10% and therefore does not change our results significantly. Particularly it cannot account for the offset of the zero-point of the Tully-Fisher relation we see for our simulated galaxies.

The angular momentum of the galaxy is calculated for the gas and stars of the galaxy as described in Paper 1, by summing over all particles, with respect to the center of mass. This angular momentum is compared to the value expected from the properties of dark matter halos $j_{\text{calc}} \approx 1.3 \times 10^3 (V_{\text{rot}}/200)^2 \text{ km s}^{-1} \text{ h}^{-1} \text{ kpc}$ as derived by Navarro & Steinmetz (2000b).

In order to study the importance of the disk in our galaxies, we also perform a dynamical decomposition following Abadi et al. (2003b). We compare the z component of the angular momentum j_z with the angular momentum of the corresponding circular orbit $j_{\text{circ}}(E)$ for each star particle. The ratio $\epsilon_j = j_z/j_{\text{circ}}(E)$ describes the degree of rotational support of a given stellar particle. A thin, rotationally supported disk has $\epsilon_j \sim 1$, a spheroid has little net rotation due to equal numbers of stars on co- and counterrotating orbits, its distribution of ϵ_j peaks at zero. All stars fitting in neither category are classified as thick disk stars. They are not rotationally supported at the same level as the thin disk, but rotate in the same manner, and spatially form a thick disk. The thin disk is generally dominated by young stars, but can also contain older stars. The dynamical bulge-to-disk ratios quoted in the tables are ratios of the mass of the bulge to the combined mass of thin and thick disk.

2.4 Comparison with observations

In order to perform a realistic comparison with observational results, particularly with respect to observed scaling relations like the Tully-Fisher relation, we create and analyze mock observations following a method described by Khalatyan et al. (2008). Using population synthesis models by Bruzual & Charlot (2003) (BC) and the software SKY-MAKER¹, we mimic observations performed by the Hubble Space Telescope. For this, the metallicity of each star particle is needed. For simplicity, in our runs without explicit

¹ Bertin & Fouqué (2007),
http://terapix.iap.fr/rubrique.php?id_rubrique=221

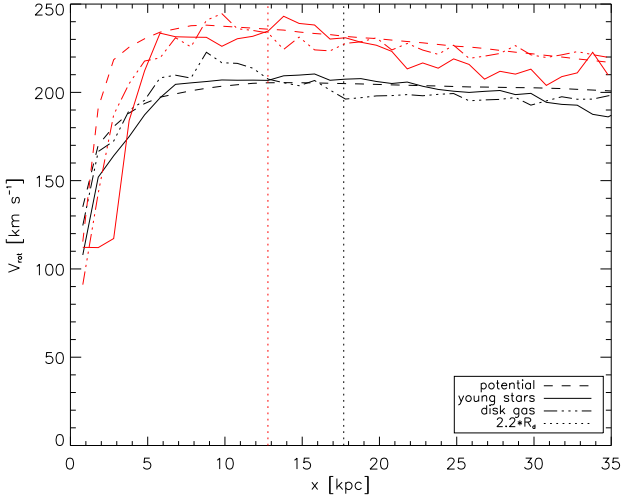


Figure 1. Rotation curves for the standard feedback model in standard (red) and high resolution (black). The long dashed line dubbed ‘potential’ is the circular velocity curve calculated from $V_{rot} = \sqrt{GM(< R)/R}$, the solid line traces the young stars in the rotationally supported disk, the dash-dotted line the cold disk gas. The vertical lines mark the location $2.2R_d$, where the rotational velocity is measured.

metal enrichment, we assume solar metallicity for star particles younger than 10 Gyr, and $Z=10^{-4}$ for star particles older than 10 Gyr. We explore BC models with Salpeter (Salpeter 1955) and Chabrier (Chabrier 2003) initial mass functions (IMF). The main difference between the two is a flatter (more physical) behavior at the low mass end for the Chabrier IMF, resulting in mass-to-light ratios being a factor of 1.5 smaller than for a Salpeter IMF. The images shown in this paper combine U, V and B band “data”. We also create I band FITS files centered on the galaxy which are used to compute the surface brightness profile using the ESO-MIDAS package², which is then fitted with GALFIT (Peng et al. 2002). To obtain the galaxy’s total magnitude as well as a photometric decomposition we fit a two component bulge+disk model to the whole profile. To find the disk scale length, we fit a pure exponential model to the outer parts. The rotational velocity is then measured with the rotation curve for the cold gas at $2.2R_d$. The I band luminosity L_I is calculated from the magnitude following Courteau et al. (2007) as $L_I=10^{-0.4(M_I-4.19)}$.

Observers measure the angular momentum of a galaxy from the rotation curve and the scale radius as $j_{obs} = 2R_d V_{rot}(2.2R_d)$. This relation, also known as the angular momentum-size relation, is inferred for an exponential disk in an isothermal halo (Fall & Efstathiou 1980). For our simulated galaxies, besides the real angular momentum content we also compute the angular momentum in this manner, using the I-band scale length and rotational velocity as described for the Tully-Fisher relation. This “exponential disk estimator” is then used to compare to the actual angular momentum to investigate possible systematics.

3 SUPERNOVA ENERGY DISTRIBUTION METHODS

In cosmological simulations, a star particle basically corresponds to a single stellar population (SSP). The energy from supernova explosions is therefore summed over the whole SSP and then distributed over the surrounding gas particles. As a first step in our investigation of supernova feedback, we study three different ways of distribution.

3.1 Implementation

We assume a Miller-Scalo initial mass function for the stellar population in one of our star particles (Miller & Scalo (1979)) with a lower cutoff of $0.1 M_\odot$ and an upper cutoff of $100 M_\odot$:

$$\xi(M) = M_\star A \begin{cases} M^{-1.25} & 0.1 < M < 1 M_\odot \\ M^{-2} & 1 < M < 2 M_\odot \\ 2^{0.3} M^{-2.3} & 2 < M < 10 M_\odot \\ 10 2^{0.3} M^{-3.3} & 10 < M < 100 M_\odot \end{cases} \quad (2)$$

where $A=0.284350751$. Stars with masses between 8 and $40 M_\odot$ explode as type II supernova, each explosion yielding an energy of 10^{51} ergs. This results in an energy of 1.21×10^{49} erg per solar mass formed. This energy is smoothed over the neighboring gas particles using the SPH smoothing kernel, so each neighbor gets an energy of

$$\Delta E_{SN,i} = E_{SN,tot} \frac{W(|\vec{r}_i - \vec{r}_\star|, h_\star) M_i}{\rho_\star} \quad (3)$$

h_\star is the smoothing length and regulates the number of gas particles receiving feedback energy. For this we try two different approaches. Initially, we use a fixed radius for the smoothing sphere of $1.37 h^{-1}$ kpc, which ensures a distribution of energy consistent with resolution. However, in this scheme, the impact of the feedback energy is highly dependent on the local density, with the same amount of energy distributed to large or small numbers of particles. The structure of the disks is improved when the size of the smoothing region scales with the local density instead, as does the smoothing length for SPH calculations in Gadget. With this scheme, the mass-weighted number of neighbors receiving feedback energy stays constant.

In the following, we briefly describe the three methods of supernova energy distribution. The *instantaneous approach* is the simplest and also most drastic method. The total supernova energy is distributed to the neighboring gas particles immediately after formation of the star particle.

Dumping the full amount of supernova energy in a single timestep is a very crude way of mimicking a real supernova remnant which expands and interacts with the surrounding ISM over an extended period of time, typically 20-30 Myr. The following two methods therefore distribute the energy more smoothly over time. In the *heat-rate approach* we distribute the energy in equal portions over a total time of $t_{SN}=20$ Myr by

$$\Delta E = E_{SN} \frac{\Delta t}{t_{SN}}, \quad (4)$$

where Δt is the current timestep of the star particle. A second possibility for a slow energy output is the *exponential approach*, an exponential feedback model using

² www.eso.org/projects/esomidas

run	M_{bar}^1	M_{bar}^2	f_{bar}	f_{cold}	SFR ³	$R_{\text{d,I}}^4$	V_{rot}^5	L_{I}^6	$(M/L)_{\star}$	B/D dyn.	B/D photo.	$j_{\text{bar}}/$ j_{calc}
MW_mr_nf	14.4	14.4	0.163	0.056	1.87	6.09	224.8	5.65	2.41	0.91	0.92	0.55
MW_mr_i	7.49	8.1	0.126	0.173	0.89	7.9	207.71	2.63	2.36	0.31	2.61	0.95
MW_mr_inc	6.17	7.53	0.141	0.127	2.52	5.85	187.46	3.27	1.62	0.57	1.84	0.9
MW_mr_h	10.7	11.0	0.136	0.119	1.12	6.18	239.37	3.82	2.52	0.75	5.06	0.48
MW_mr_hnc	7.07	8.91	0.146	0.079	3.86	5.36	186.67	4.23	1.48	0.42	0.14	0.86
MW_mr_e	10.05	10.55	0.134	0.119	1.51	7.81	221.06	3.66	2.47	0.5	2.48	0.71
MW_mr_enc	8.05	8.7	0.136	0.094	1.31	7.03	221.2	3.3	2.21	0.35	0.59	0.7
MW_mr_encv	10.4	10.8	0.143	0.104	2.55	6.01	243.1	4.63	2.08	0.43	0.27	0.62
MW_hr_encv	7.2	7.82	0.113	0.11	1.38	7.89	207.47	3.13	2.06	1.02	1.49	0.9

Table 2. Characteristic parameters for the galaxies with different distribution methods for the feedback energy. V_{rot} is measured for young stars at $2.2R_{\text{d,I}}$. The luminosity and mass-to-light ratio are based on a Chabrier IMF for the edge-on projection. The last column measures the angular momentum content and contains the ratio of the total angular momentum of stars and gas in the galaxy and the expected value based on the relation $j_{\text{calc}} \approx 1.3 \times 10^3 (V_{\text{rot}}/200)^2 \text{ km s}^{-1} \text{ h}^{-1} \text{ kpc}$ from Navarro & Steinmetz (2000b).

¹ galaxy mass including cold gas only, in $10^{10} M_{\odot}$; ² galaxy mass including all gas, in $10^{10} M_{\odot}$; ³ in $M_{\odot} \text{ yr}^{-1}$; ⁴ in kpc; ⁵ in km s^{-1} ; ⁶ in $10^{10} L_{\odot}$

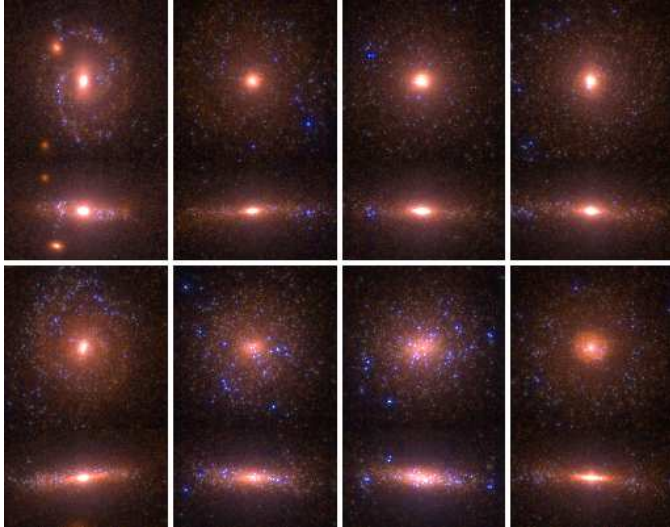


Figure 2. Mock observations in face on and edge on projections of our simulated galaxies with different methods of distributing feedback energy as described in the text and in Table 2. Each box has a side length of 60 kpc, and those with the edge-on projection a height of 30 kpc. In the top row we have the model without feedback, the instantaneous model, the heat-rate model and the exponential model. The models in the bottom row correspond to those on the top, but with cooling locally turned off. The bottom left panel is our standard model (exponential with local cooling turnoff and variable smoothing length).

$$\Delta E = E_{\text{SN}} \frac{t - t_{\star}}{t_{\text{SN}}} e^{-\frac{t-t_{\star}}{t_{\text{SN}}}} \frac{\Delta t}{t_{\text{SN}}}. \quad (5)$$

Again, $t_{\text{SN}}=20 \text{ Myr}$ and t_{\star} is the formation time of the stellar particle. This model mimics effects owing to the formation time and lifetimes of stars with different masses.

We also test variations of all of these methods where radiative cooling is turned off temporarily in the gas particles

receiving supernova energy (Gerritsen 1997). This helps to prevent immediate re-radiation of the thermal energy due to the high density of the gas surrounding the star formation sites and the inability to resolve the multiphase structure of the interstellar medium. We choose a turnoff time period of 20 Myr, based on typical cooling times for supernova blast-waves. With this we attempt to suppress the strong early star formation more efficiently.

3.2 Results

Table 2 and Figure 2 give an impression of the results for the different energy distribution methods. Our standard halo MW_mr has been used as initial conditions for all of these runs. The abbreviations i (=instantaneous), h (=heat-rate) and e (=exponential) indicate the type of feedback, nc stands for the local cooling turnoff, and nf for no feedback which is a run with only star formation which is included for comparison. All runs are employing fixed smoothing length except one, MW_mr_encv, with variable smoothing length for feedback energy. Variable in this case means that the smoothing length is calculated following the smoothing length for the SPH density calculation. It is scaled according to the mass-weighted number of neighbors which is kept constant to a value of 40. We experimented with the variable smoothing length also in the other cases but could not see substantial improvement. The first obvious result from Figure 2 is the importance of turning off the cooling locally in order to form a young, bright disk (bottom row vs top row). This is also clear from the stellar surface density profiles shown in Figure 3. While all runs with feedback are quite similar outside of about 8 kpc, the galaxies with the cooling turn-off have a much flatter slope in the inner regions, corresponding to a smaller bulge. In the simulation without any feedback, the bulge is most dominant, as is expected. The two prominent spiral arms seen in the image in the top left panel of Figure 2 are due to ongoing mergers of

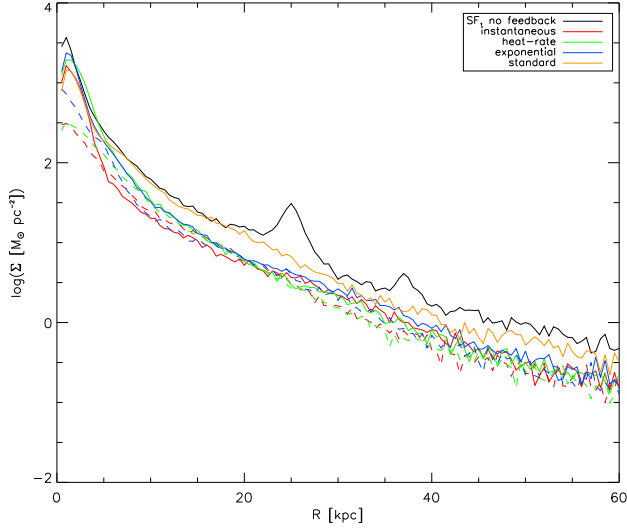


Figure 3. Stellar surface density profiles for the different feedback models. The different colors indicate the different models as shown in the legend. The dashed lines show the corresponding model with local cooling turned off. The bump in the model without feedback and in the exponential model at about 25 kpc radius corresponds to an incoming satellite galaxy also clearly visible in Figure 2.

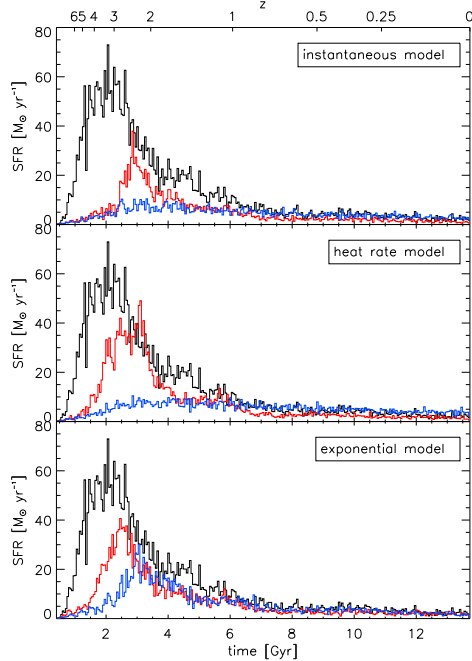


Figure 4. Comparing the star formation histories for the different feedback energy distribution methods in comparison to the run without feedback (black line). The red line shows the standard case, the blue line the case with locally turned off cooling (“nc”).

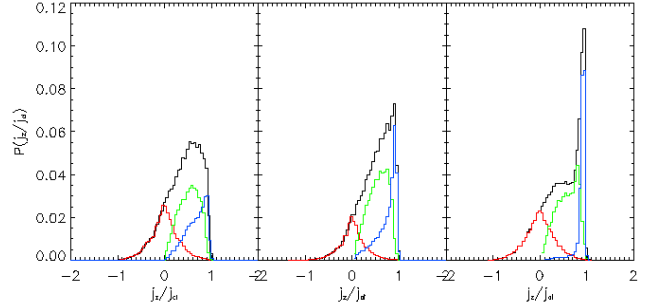


Figure 5. Dynamical decomposition of the stellar component for the heat rate model (left panel), the heat-rate model with variable smoothing length (middle panel) and the exponential model with exponential smoothing length (right panel), all with local cooling turn-off. The black line represents all stars, the blue line thin disk stars, the green line thick disk stars and the red line the spheroidal component.

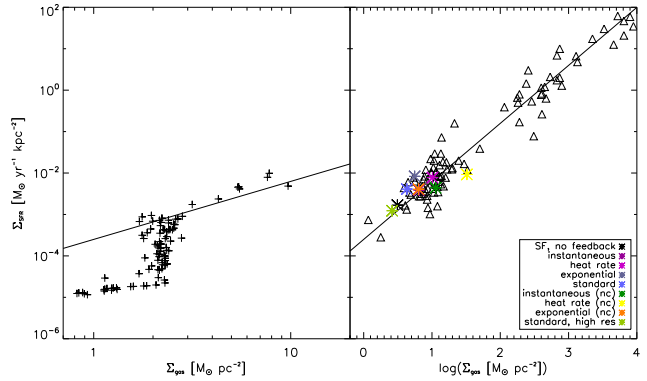


Figure 6. Left panel: Agreement of the galaxy formed in the standard high resolution model with the Kennicutt law, locally given by equation 6 (solid line). In the outer region, the star formation rate drops since the disk is no longer Toomre instable. Right panel: Agreement of all our galaxies with different feedback distribution methods with the observed global Kennicutt law. The triangles are observational data points from Kennicutt (1998). Our model galaxies populate the lower surface density region in agreement with the regular galaxies, while the observed galaxies with high surface densities are starburst galaxies.

smaller satellites (one is also visible in the image) inducing new star formation. Nevertheless the galaxy is very massive, slowly rotating and clearly spheroidal with a very low angular momentum. The clearly visible incoming satellite can be seen as a bump in the surface density profile. The bulge is also important in runs with feedback but without the local cooling turn-off.

Figure 4 shows the star formation histories for all cases in comparison with the no-feedback run. We see that the instantaneous model even without the local cooling turn-off suppresses early star formation most efficiently due to the instantaneous energy input. The star formation history for the two models with smooth energy input are very similar, except when cooling is turned off locally, which has less influence in the exponential model than in the heat-

rate model. However, in the basic instantaneous model, star formation is suppressed but not self-regulated which is why we do not see a young stellar disk. The feedback actually becomes too strong. When we turn off cooling locally, a significant amount of gas stays hot for a longer amount of time, but also close to the disk, so when it cools again it can form stars there and we find a young but rather thick and unstructured stellar disk. In the exponential model, the suppression is less efficient and the young disk less prominent.

A more prominent spiral structure is achieved when a variable smoothing length is used, since in that case the code can better adjust to local density structures. For the exponential model with cooling turnoff this is shown in the bottom left image of Figure 2. Our two best cases in comparison to the Milky Way are MW_mr_hnc and MW_mr_encv, i.e. the heat-rate and the exponential model with local cooling turnoff and, for the latter, with a variable smoothing length. MW_mr_hnc has an almost perfect exponential surface brightness profile and is almost not angular momentum deficient. Nevertheless, as shown in Figure 5, the dynamic decomposition shows it to be rather a thick disk instead of a thin disk and a bulge, and the structure of the disk is very clumpy. This does not improve much when a variable smoothing length is used in this case. We therefore select MW_mr_encv as our standard model for the rest of our work. It fits the Kennicutt relation, given by

$$\Sigma_{\text{SFR}} = (1.5 \pm 0.7) \times 10^{-4} \left(\frac{\Sigma_{\text{gas}}}{\text{M}_{\odot} \text{pc}^{-2}} \right)^{1.4 \pm 0.15} \frac{\text{M}_{\odot}}{\text{yr kpc}^2}, \quad (6)$$

well as shown in the left panel of Figure 6, though the outer regions are no longer Toomre unstable and the star formation density drops. In general, all of our models fall well within the scatter of the observed global Kennicutt relation in the region of regular galaxies, as shown in the right panel of Figure 6.

We test the standard model with our higher resolution halo, as run MW_hr_encv, with about 10^6 gas, star and dark matter particles within the virial radius. Our feedback method does depend somewhat on resolution with the main effect being a more efficient suppression of star formation which reduces the total galaxy mass as measured in a radius of $6R_d$ by about 30%. The high resolution galaxy has basically no angular momentum deficiency. Even though the scale length in the high resolution case is a little larger, the surface brightness profiles are very similar. Overall the higher resolution is slightly different in some aspects but the model is reasonably robust and the changes at higher resolution improve the disk rather than having a negative impact.

4 INFLUENCE OF DIFFERENT ASSEMBLY HISTORIES

Owing to the persistent problem of forming realistic disk galaxies in cosmological simulations over the past two decades, it became custom to choose a halo with what is thought to be favorable conditions for the formation of a disk. This comprises particularly a high spin parameter, resulting in disks with large scale lengths, and no late large mergers which could destroy the disk. The goal is to succeed in simulating at least one good disk as a basis

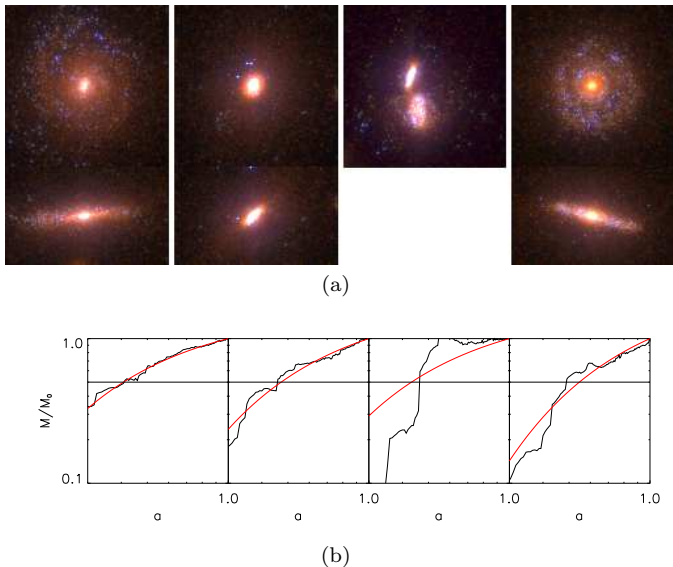


Figure 7. Panel (a): Mock observations of the Milky Way type galaxies with different merging histories, all run with the standard feedback model. For comparison the standard halo is shown on the left, followed from left to right by MW_mh1_mr, MW_mh2_mr and MW_mh3_mr. There is no edge-on projection for MW_mh2_mr, since this is still in the process of merging. Panel (b): The halo mass growth in dependence of the scale parameter a , fitted with the model given by Equation 7 to assess how typical the halo is.

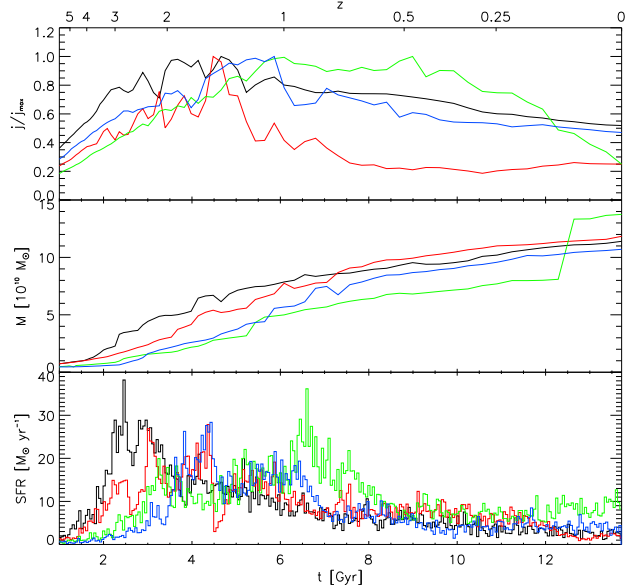


Figure 8. The angular momentum evolution (top panel) and mass growth (middle panel) for the combined stellar and gaseous components, and the star formation history (bottom panel) of the galaxies in halos with different assembly histories. The lines (black, red, green and blue) correspond to the halos as shown in Figure 7(a) from left to right, with the black line being our standard halo.

for further work. However, it has been shown recently by Scannapieco et al. (2009) that disks can form in a whole range of halos with high or low spin parameters leading these authors to question the previously assumed correlation between formation history and morphology of a galaxy. Governato et al. (2008) showed that an extended disk can form in a simulation even after larger mergers via re-growth, if the progenitors are gas-rich. We therefore also apply our standard feedback model to three other halos with a similar Milky Way-type mass as the standard halo, but with different merging histories. The only criterion in picking these halos was their mass and a distance of at least 2 Mpc h^{-1} to the next object of equal or higher mass in order to avoid direct encounters at $z=0$. In Table 1 these are the runs denoted by MW_mh1_mr, MW_mh2_mr and MW_mh3_mr. The assembly histories and mock observations are shown in Figure 7. To characterize, how typical the chosen halos are, we fit the mass growth curve using

$$M(a) = M_0 e^{-\alpha z}, \alpha = (1+z)^{-1} \quad (7)$$

from Wechsler et al. (2002) (α is a free parameter characterizing a characteristic epoch of formation). For mass accretion histories without large mergers, this provides a good description. This is the case for our standard halo, for MW_mh1_mr and also, with some limitation, MW_mh3_mr, as can be seen in Figure 7(b).

Figure 8 shows the angular momentum, mass growth and star formation history of the galaxies compared to our standard halo. MW_mh2_mr is a quite extreme case. Two large baryonic progenitors merge at $z \approx 0.1$, and as is obvious in the image in Figure 7(a), this process is not finished at $z=0$. The plot of the mass growth of the halo shows only a very slight increase at these late times, after a very large (1.26:1) merger at around $z=1$. The merger coincides with a large starburst.

Comparing the assembly histories of MW_mh1_mr and MW_mh3_mr, we would have expected MW_mh1_mr to be more likely to have a disk, due to the large mass increase at $z=1$ for MW_mh3_mr (where the mass is more than doubled; this is preceded by a 3.14:1 dark matter merger). However, as can be seen from the angular momentum evolution in Figure 8, the assembly is more chaotic for MW_mh1_mr with a very large loss of angular momentum at $z \approx 1.3$ coinciding with a drop in star formation. After that, even though the disk still grows in mass, it does not in size. At $z=1$ it already resembles very closely its final state. It is a low angular momentum system with $\lambda = 0.023$, compared to $\lambda = 0.05$ for MW_mh3_mr. The latter, despite its later merger, loses significantly less angular momentum in its merger. The angular momentum evolution and mass growth are both quite comparable to our standard model except for the delayed assembly. While in radius it is comparable to MW_mh1_mr at $z \approx 1$, its disk can grow due to higher angular momentum gas still entering the system. Also, star formation sets in much later for this halo, peaking at $z \approx 1.5$ instead of 3 as in the standard model, due to the overall later assembly (see Figure 8). This helps in keeping the bulge small. Star formation is generally slightly higher for MW_mh1_mr (with $10 \text{ M}_\odot \text{ yr}^{-1}$ from $z \approx 1$ to $z \approx 0.25$), leading to a low final gas fraction of 0.015 compared to 0.084 for MW_mh3_mr, and overall to a much more spheroidal shape.

We can conclude that a quiet and early assembly history of the dark matter halo does not necessarily lead to a disk, confirming the conclusions by Scannapieco et al. (2009). Not only the time of the last major merger, but rather the onset of star formation and the impact particularly in loss of angular momentum seems to mainly influence the disk. This could be related to the geometry of the merging disks as suggested by Scannapieco et al. (2009). The quick growth of the disk in our MW_mh3_mr halo is very similar to what has been reported by Governato et al. (2008).

5 THE STANDARD MODEL OVER A RANGE OF MASSES

To test the performance of our standard model with respect to the observed scaling relations of disk galaxies, we perform runs using halos spanning a mass range from 1.13×10^{11} to $1.94 \times 10^{12} \text{ M}_\odot$ in dark matter halo virial mass. For all except the largest mass halo, we have performed the runs with an effective resolution of 2048^3 ("hr" runs in our nomenclature). The halos were selected to have no late major mergers as well as relatively high spin parameters. The latter did not necessarily impact the disk. The galaxies forming in the halos DM_hr3 and DM_hr7 are not very disk-like. While the latter indeed has a rather low spin parameter with $\lambda = 0.018$, the spin parameter of the former is $\lambda = 0.034$, quite close to the mean value of halos. All of the chosen halos have a fairly quiet assembly history. The gallery of mock observations for these runs is shown in Figure 9, with increasing mass from top left to bottom right and the standard halo in high resolution being the third image in the bottom row. Table 3 contains the characteristic parameters.

In our sample we have two very good cases with a strong rotationally supported young thin disk: DM_hr2 ($M_{\text{halo}} = 2.52 \times 10^{11} \text{ M}_\odot$) and DM_hr6 ($M_{\text{halo}} = 7.03 \times 10^{11} \text{ M}_\odot$), but their masses are too low to resemble the Milky Way. While DM_hr2 has a fairly constant star formation history (SFH) of about $1.75 \text{ M}_\odot \text{ yr}^{-1}$, the other halos tend to have a series of bursts showing the self-regulation of the feedback model. The surface brightness profiles of the rotationally supported disks are very close to exponential, which can also be seen from their low photometric bulge-to-disk (B/D) ratios showing a bright and prominent disk. For DM_hr6, this is 0.53, the lowest of the set. Dynamically, the bulge tends to be stronger except for DM_hr2, where $(B/D)_{\text{dyn}} = 0.27$ only. Our highest mass halo does not host a disk galaxy, but a very luminous object. Possibly due to the lower resolution it was simulated with, the disk never really grows to an appreciable size. Therefore it is not expected to follow the scaling relationships for disk galaxies, as will be confirmed in the following section. This result is not surprising, since observationally, the most luminous galaxies are indeed elliptical galaxies.

5.1 Comparison with observed scaling relations

The most important observed scaling relations with which one can test simulations of disk galaxies are the Tully-Fisher relation, the baryonic Tully-Fisher relation and relations with respect to the angular momentum. We will discuss all of these in the following sections.

run	M_{bar}^1	M_{bar}^2	f_{bar}	f_{cold}	SFR	$R_{\text{d,I}}$	V_{rot}	L_{I}	$(M/L)_{\star}$	B/D dyn.	B/D photo.	$j_{\text{bar}}/$ j_{calc}
DM_hr1	0.95	0.97	0.11	0.326	0.3	3.26	105.44	0.39	1.93	2.23	0.25	0.83
DM_hr2	2.44	2.49	0.134	0.135	1.75	3.81	136.92	1.5	1.41	0.27	0.69	0.9
DM_hr3	2.8	2.84	0.124	0.158	0.77	3.43	156.06	1.31	1.89	0.86	3.37	0.4
DM_hr4	4.07	4.13	0.111	0.112	1.17	3.6	186.49	1.86	1.98	0.5	0.68	0.31
DM_hr5	4.57	4.62	0.113	0.09	1.52	3.01	199.01	2.35	1.8	2.06	1.38	0.29
DM_hr6	5.38	5.54	0.119	0.168	1.75	5.08	194.81	2.58	1.8	0.91	0.53	0.67
MW_hr	7.2	7.82	0.113	0.11	1.38	7.89	207.47	3.13	2.06	1.02	1.49	0.9
DM_mr7	1.75	1.8	0.137	0.048	6.7	3.48	319.64	8.73	1.91	0.42	0.56	0.09

Table 3. Characteristic parameters for the resulting galaxies in the standard model applied to halos of increasing masses. ¹ galaxy mass including cold gas only, in $10^{10} M_{\odot}$; ² galaxy mass including all gas, in $10^{10} M_{\odot}$; ³ in $M_{\odot} \text{ yr}^{-1}$; ⁴ in kpc; ⁵ in km s^{-1} ; ⁶ in $10^{10} L_{\odot}$

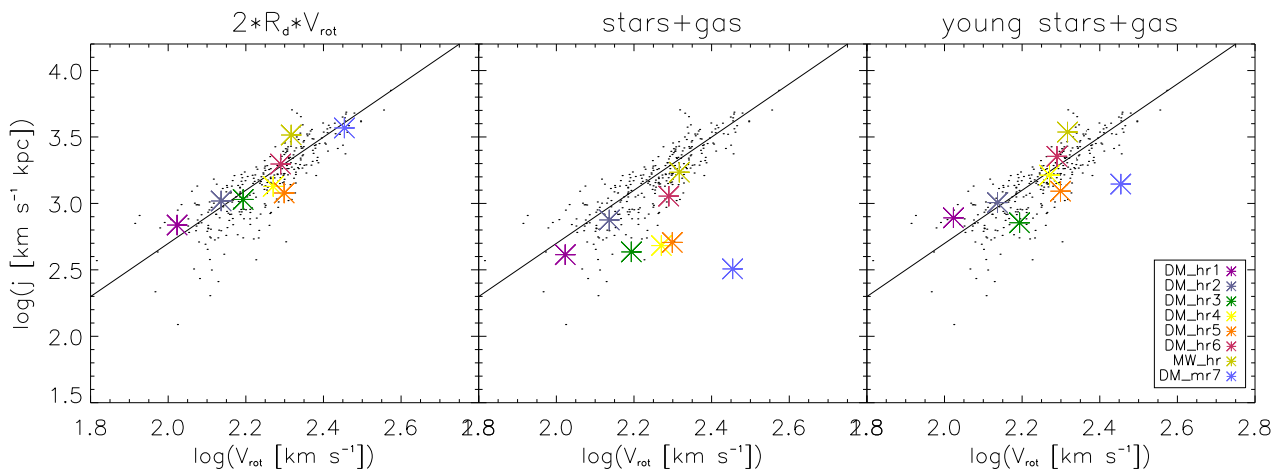


Figure 10. Comparing the simulated galaxies to the observed angular momentum relation (dots), well fitted by the prediction from Navarro & Steinmetz (2000b) (line). The left panel shows the angular momentum-size relation, the middle panel the true angular momentum of gas and stars in the simulated galaxies, and the right panel the angular momentum of the rotationally supported disk of young stars and gas.

5.1.1 The angular momentum relations

For the angular momentum, we discuss two relations: the angular momentum-size relation (as the “exponential disk estimator” from Section 2.4) and the relation of the rotational velocity with the actual angular momentum of the galaxy. Our methodology to measure the scaling length, rotational velocity, and angular momentum is described in Section 2. We compare with observed data from Giovanelli et al. (1997). Figure 10 shows the two relations. The solid line is the expected relation (based on halo properties) from Navarro & Steinmetz (2000b), $j_{\text{calc}} = 1300(V_{\text{rot}}/200)^2 \text{ km s}^{-1} \text{ h}^{-1} \text{ kpc}$. The left panel shows the angular momentum-size relation. Since the rotation curves of disks are mostly flat, this translates to a measure for the extend of the disk. For this we calculate j using $j = 2R_{\text{d}}V_{\text{rot}}$ (Mo, Mao & White 1998). The disk sizes of our simulated galaxies are well within the observational scatter

of the relation. The only outlier is, as expected, DM_hr7. Our disks therefore do not suffer from being too compact and centrally concentrated, as in earlier simulations. Looking at the middle panel, which plots the actual angular momentum content of gas and stars in the galaxy, we see that even though our galaxies tend to be slightly below the expected relation, again they fall within the observed scatter. DM_hr1, DM_hr2, MW_hr and also DM_hr6 have almost no angular momentum deficiency, while DM_hr5 is quite deficient due to a large amount of counterrotating gas. If we only look at the actual disk consisting of cold gas and young stars, our data scatter right around the expected relation. The difference between the angular momentum as calculated from $j = 2R_{\text{d}}V_{\text{rot}}$, the exponential disk estimator, and the actual angular momentum content could be equivalent to a systematic difference between angular momentum measured by observers and angular momentum derived from simulations. This prompted us to compare these values directly, as

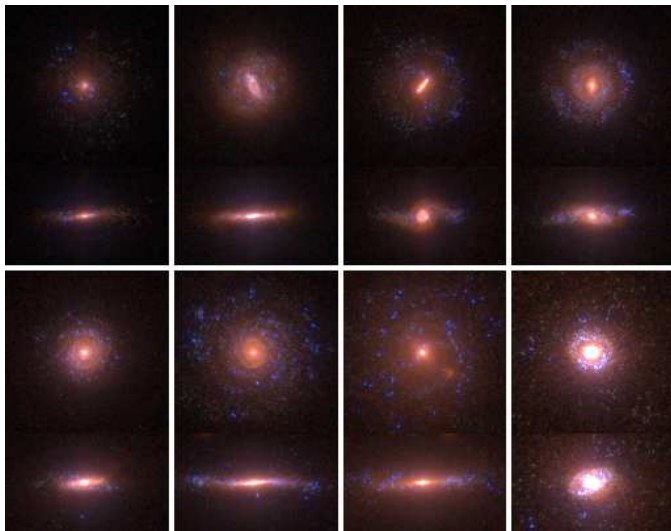


Figure 9. Mock observations of runs of halos spanning a mass range of an order of magnitude, from 1.13×10^{11} to $1.94 \times 10^{12} M_{\odot}$ in dark matter halo virial mass. The top row shows runs DM_hr1, DM_hr2, DM_hr3 and DM_hr4, the bottom row has DM_hr5, DM_hr6, MW_hr (the standard run in high resolution) and DM_mr7, the only one in this set with the medium resolution of 1024^3 effective resolution.

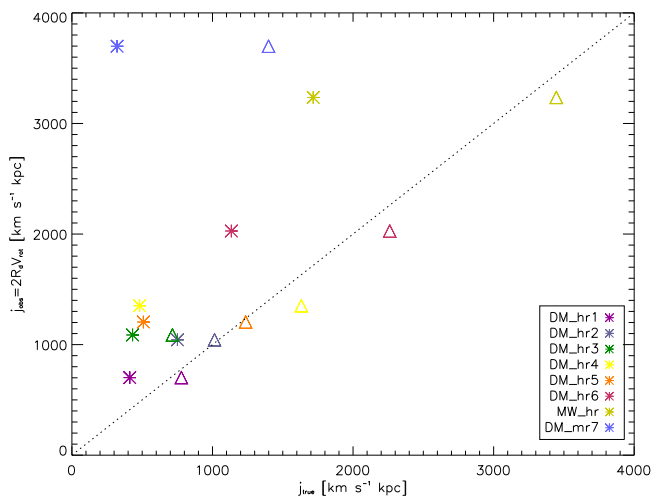


Figure 11. The true, directly measured angular momentum of the simulated galaxies vs. the exponential disk estimator $2R_d V_{rot}$. The dotted line indicates a direct correspondence. The star symbols are for the angular momentum of the whole galaxy, the triangles for the disk (gas and young stars) only.

shown in Figure 11. We indeed see a clear offset for the total angular momentum content, while the angular momentum of the *disk* (i.e. of disk gas and young stars) is directly correlated with the ‘observed’ values. Two conclusions arise from this. First, a fair comparison between observations and simulations with respect to angular momentum is not straightforward when the simulated galaxies have large bulge components. This is the case for those of our galaxies which show the largest difference, DM_hr3, DM_hr4 and DM_hr5.

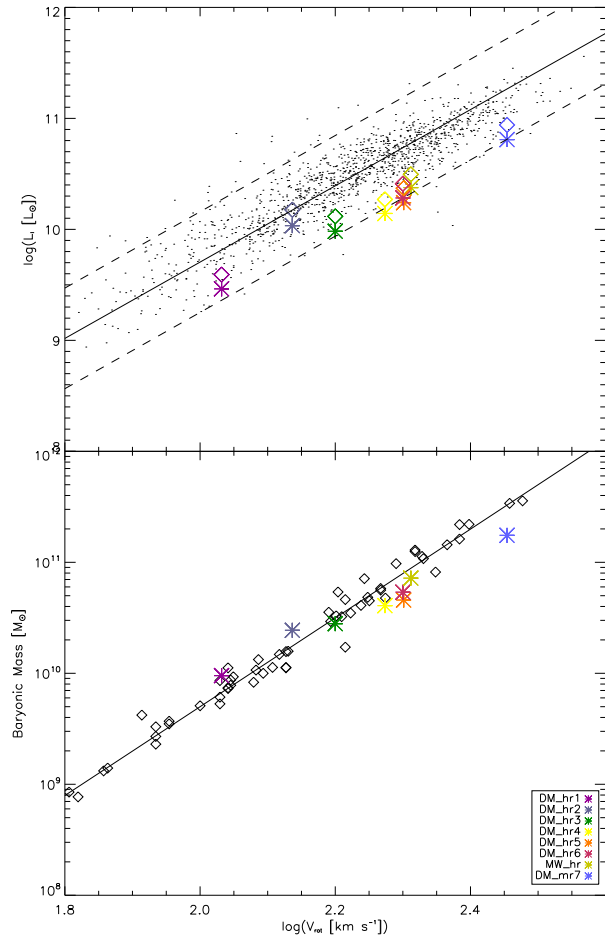


Figure 12. The I-band (top) and baryonic (bottom) Tully-Fisher relations for our halos of different masses. The black points in the top panel are observations from the sample of Courteau et al. (2007). The solid line is a fit, the dashed lines the 2σ observed scatter. The stars are for a Salpeter IMF, the diamonds for a Chabrier IMF for our simulated galaxies. In the bottom panel, the black diamonds are observational data from McGaugh (2005) with a fit shown again by the solid line.

Our standard feedback model is not able to produce a bulge-less disk and only one clearly dominated by a disk, DM_hr2 with $B/D=0.27$. The second conclusion is that our actual disks composed of young stars and cold gas have kinematic characteristics of real disks.

5.1.2 The Tully-Fisher Relation

The Tully-Fisher relation is one of the fundamental benchmarks for a successful model of disk formation, and one of the biggest challenges of simulations, since so far it remains difficult to reproduce the slope and the zero-point of the observed relation. It relates the rotational velocity with the total luminosity of the galaxy and is most often measured in the I or K-band since this is most representative of the total stellar mass. We compare our results to observations compiled by Courteau et al. (2007). The relation is of type $L \propto V^\alpha$ and their fit to the $\log V$ vs. $\log L_I$ plot gives a

slope of 0.291 ± 0.004 and a zero point of -0.835 ± 0.039 with a scatter $\sigma_{\ln V|L} = 0.132$. The top panel of Figure 12 shows our data overplotted on this relation. Our standard model misses the zero point of the relation by being too faint by about a magnitude when a Salpeter IMF is used. The simulated galaxies barely fall within the scatter. The only exception is the galaxy in halo DM_hr2 which comfortably lies within the scatter, though still below the best fit relation by half a magnitude. A slight improvement can be achieved when using a Chabrier IMF, shown by diamond symbols in Figure 12, but for most galaxies the discrepancy is still large.

The most fundamental relation to which the Tully-Fisher relation can be traced is the baryonic Tully-Fisher relation (see McGaugh 2005) relating rotational velocity to total baryonic mass. We compare to it in the bottom panel of Figure 12. McGaugh (2005) finds as best fit to his observations the relation $M_{\text{bar}} = 50V_{\text{rot}}^4$. All simulated galaxies are well within the observed scatter. We seem to get a slightly shallower relation, though we do not really have enough data points for a fit and the low mass halos also might be influenced by resolution effects. With the exception of our expected outlier, DM_mr7, we find the agreement to be quite good.

From the results of the scaling relation comparisons we conclude that our model is able to produce galaxies which are correct structurally, but still bulge dominated and not luminous enough. Our I band stellar mass-to-light ratios of $M/L \approx 2$ (for a Chabrier IMF) are improved compared to earlier simulations for example by Navarro & Steinmetz (2000b) (who had $M/L \approx 2.5$), but are still too high compared to analytical expectations based on Mo, Mao & White (1998) in combination with the observed Tully-Fisher relation which yield $M/L \approx 1-1.5$. We suspect this to be the main reason for the failure in fitting the Tully-Fisher zero point, rather than an incorrect rotational velocity due to peaked rotation curves. Another effect could be that the concentration of the dark matter halo is too high resulting in too high rotational velocities (Navarro & Steinmetz 2000a).

6 INCLUDING ADDITIONAL PHYSICAL PROCESSES

The physical processes playing a role in the formation and evolution of a galaxy are much more complex than just simple star formation and energy feedback. In this section we describe a number of other relevant physical effects we tested to study their influence on our standard model galaxy. An overview of the characteristic parameters of the resulting galaxies can be found in Table 4, and Figure 13 gives a visual impression of the results.

6.1 Implementation

Before discussing the results we first briefly describe the implementation in each case. The abbreviation in brackets is used later when referring to the simulations.

- (i) A UV background (*UV*)

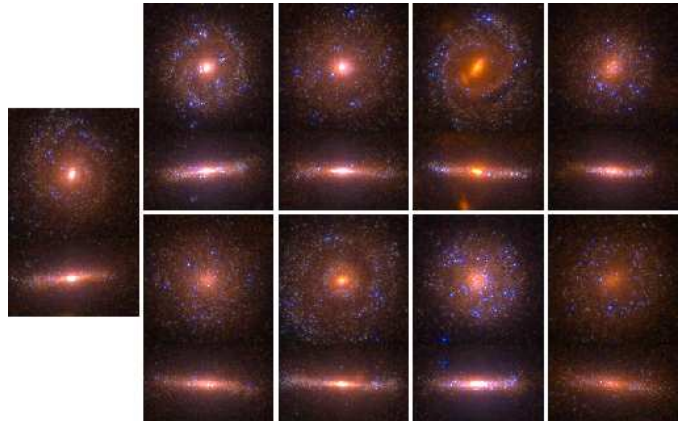


Figure 13. Mock observations of the galaxies run with the standard feedback model and different additional physics effects. For comparison the standard model itself is shown on the left. The top row shows the runs with UV background, type Ia supernovae, metal-dependent cooling and the "all in" model with metal-dependent cooling. In the bottom row we show the runs with 10% kinetic feedback, mass return, the "all in" model and the blastwave model.

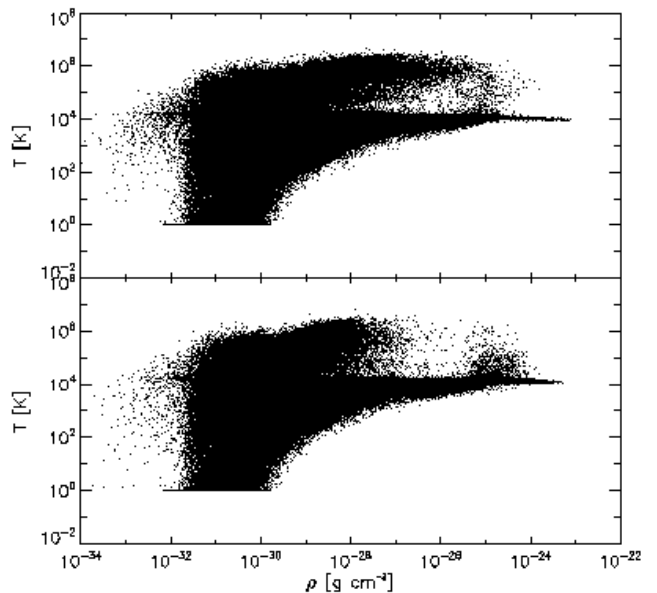


Figure 14. Metal-dependent cooling clearly reduces the amount of hot gas in the halo (bottom panel) compared to the standard run (top panel). According to our definition for the size of the halo, gas with $\rho > 9.29 \times 10^{-28} \text{ g cm}^{-3}$ belongs to the halo.

An external ultraviolet background is included in the Gadget2 cooling routine available to us from Volker Springel. It is a modified Haardt & Madau (1996) spectrum with reionization at $z \sim 6$ (Davé et al. 1999).

- (ii) Kinetic feedback (*kin*)

In order to stimulate the generation of winds by supernova explosions we test a model of splitting the supernova energy into a thermal and a kinetic feedback component. The ratio is governed by a parameter $f_v = E_{\text{kin}}/E_{\text{SN}}$, which

run	M_{bar}^1	M_{bar}^2	f_{bar}	f_{cold}	SFR	$R_{\text{d,I}}$	V_{rot}	L_{I}	$(M/L)_{\star}$	B/D dyn.	B/D photo.	$j_{\text{bar}}/$ j_{calc}
standard	10.4	10.8	0.143	0.104	2.55	6.01	243.1	4.63	2.08	0.43	0.27	0.62
UV	9.64	11.0	0.165	0.056	4.07	5.74	218.02	5.22	1.74	0.41	1.79	0.65
kin	7.25	7.88	0.118	0.15	2.14	6.56	202.71	3.35	1.83	0.38	0.47	1.0
SNI	11.2	12.3	0.154	0.086	2.5	6.74	240.27	5.02	2.05	0.18	0.67	0.71
met	10.5	11.1	0.137	0.139	2.77	7.89	223.15	4.65	1.96	0.42	3.73	0.89
mSN	10.8	11.9	0.151	0.118	2.67	7.01	236.27	4.72	2.05	0.33	3.66	0.73
metc	15.2	15.3	0.164	0.105	1.64	7.07	242.34	5.41	2.57	0.33	2.75	0.64
bl	5.97	6.64	0.144	0.132	0.98	7.82	185.22	2.33	2.2	0.46	0.82	1.21
all in	9.59	11.1	0.157	0.154	5.7	5.67	225.15	5.6	1.51	0.26	1.17	0.78
all in, mc	7.5	7.52	0.09	0.162	1.85	5.08	204.28	3.24	1.97	0.44	1.01	0.72

Table 4. Characteristic parameters for the resulting galaxies in the standard model with different additional physical effects. The standard model MW_mr_envc is shown again for comparison in the top row.

¹ galaxy mass including cold gas only, in $10^{10} M_{\odot}$; ² galaxy mass including all gas, in $10^{10} M_{\odot}$; ³ in $M_{\odot} \text{ yr}^{-1}$; ⁴ in kpc; ⁵ in km s^{-1} ; ⁶ in $10^{10} L_{\odot}$

we set to 10%. We follow a “momentum” approach as in Navarro & White (1993), where the velocity of the neighboring gas particles is changed via

$$\Delta v_j = \sqrt{\frac{2f_v E_{SN}(t)}{\sum m_j}}. \quad (8)$$

(iii) Type Ia supernovae (*SNI*)

Type Ia supernovae arise from binary systems with a total mass of 3-16 M_{\odot} and are particularly important for a delayed input of feedback energy as well as for metal enrichment since they are a main source for iron. We implement them following Scannapieco et al. (2006), assuming a progenitor lifetime between 0.1 and 1 Gyr. The exact time for energy (and metal) injection is chosen randomly from this range. The relative supernova rate of type Ia to type II is estimated from observations as 0.245 (Cappellaro et al. (1999), for a Milky Way type galaxy (type Sbc) with $L_B(\text{MW}) = 2.3 \times 10^{10} L_{\odot}$). Each type Ia supernova is assumed to have an energy of 10^{51} ergs and we do not disable the cooling locally for these events (following Stinson et al. 2006).

(iv) Mass return (*met* & *mSN*)

In this model we return mass to neighboring gas particles in the same way as energy, smoothing it via the SPH Kernel. This should not have a big influence, but results in stars of different masses and therefore different amounts of returned feedback energy. This is also required to track metal enrichment which we do using oxygen and iron. For type II supernovae we use yields from Woosley & Weaver (1995) taking into account the dependence on metallicity for the iron yields. To get more realistic abundances, one has to include type Ia supernovae, since they are mostly responsible for the iron production. For this we use yields from Raiteri et al. (1996) which are based on Thielemann et al. (1998) and are independent of the progenitor mass. This is a separate model (*mSN*), since the energy of type Ia supernovae is an additional factor.

(v) Metal-dependent cooling (*metc*)

The metal abundance in the gas has a strong influence on the strength of the cooling. At a temperature of 10^5 K , primordial gas will have a cooling time which is about 50 times longer than gas with $[\text{Fe}/\text{H}]=0.5$ (Sutherland & Dopita 1993). This results in a decreased amount of hot gas around the halo, as shown in Figure 14 in comparison to the standard run. Despite its importance, most current simulations do not include this effect (exceptions are Abadi et al. (2003a), Scannapieco et al. (2006), Okamoto et al. (2005) and Kawata & Gibson (2005)). Based on our crude model of metal enrichment described above, we include metal-dependent cooling by interpolating the tables of Sutherland & Dopita (1993) which cover, besides the primordial case, the abundances $[\text{Fe}/\text{H}]=\{-3.,-2.,-1.5,-1.,-0.5,0,0.5\}$ and a temperature range of $4 \leq \log(T) \leq 8.5$. For values outside these ranges, the respective extremes are used.

(vi) Blastwave feedback (*bl*)

In our standard model using the SPH based method of smoothing energy and mass over neighboring gas particles with a variable-sized smoothing sphere, this size is computed so that the enclosed mass in the sphere is constant. This is numerically more sensible than our first attempt of using a fixed (albeit physically motivated) radius of 1.37 kpc h^{-1} . However, it is not very closely connected to the underlying physics it is supposed to represent. To improve on this, we implemented a version of the blastwave feedback suggested by Stinson et al. (2006). In this model, the size of the smoothing sphere and also the time span for which cooling should be turned off are not free parameters, but calculated through the explicit blastwave solution based on Chevalier (1974) and McKee & Ostriker (1977). The blastwave radius is given by

$$R_E = 10^{1.74} E_{51}^{0.32} n_0^{-0.16} \tilde{P}_{04}^{-0.2} \text{ pc} \quad (9)$$

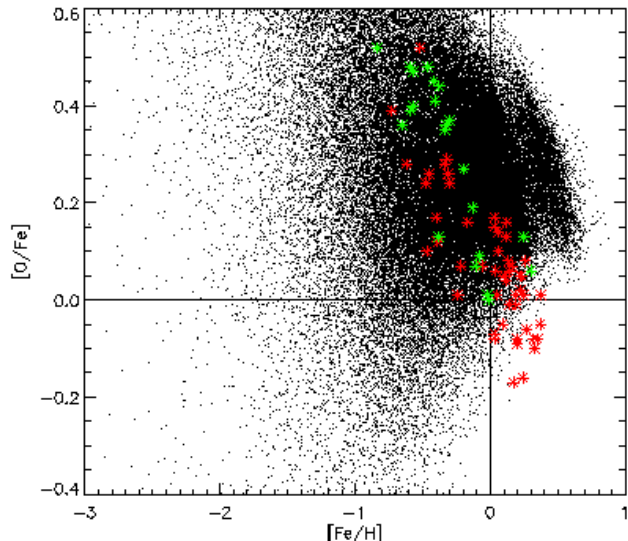


Figure 15. Oxygen abundance in relation to iron for our stars in the standard model (black dots) compared to observational data from the Milky Way by Bensby et al. (2004). The green points are thick disk and the red points thin disk stars. Our simulation is in reasonable agreement with the former, though underabundant in iron.

and the timescale (i.e. the time until which cooling is disabled) is

$$t_E = 10^{5.92} E_{51}^{0.31} n_0^{0.27} \tilde{P}_{04}^{-0.64} \text{yr} \quad (10)$$

with $E_{SN} = E_{51} 10^{51}$ ergs and $\tilde{P}_{04} = 10^{-4} P_0 k^{-1}$. P_0 and n_0 are the ambient pressure and hydrogen density. We here use as time t_E the time until the end of the snowplow phase, another option would be the time until the hot, low density shell survives. Stinson et al. (2006) found no significant difference between the two. Following Stinson et al. (2006) we distribute feedback energy to gas particles within R_E , but mass and metals (if turned on) within the original smoothing radius.

6.2 Results

From the visual impression of Figure 13 it seems that all of the additional physical effects except the blastwave method help to make the galaxy younger and brighter. This is caused by a further suppression of star formation early in the assembly history, leaving more gas for later star formation. The blastwave method also causes such a suppression, but in this case we additionally have a later onset of star formation and a peak reduced to $9 M_\odot \text{yr}^{-1}$ at $z \sim 1.5$. Still, despite much fewer stars and therefore less feedback activity, this feedback is strong enough to result in the lowest galaxy mass of all cases, with only 60% of the mass in the standard case. Photometrically the bulge is strongly reduced and the galaxy also has the lowest luminosity and current star formation rate of all models. Dynamically it is more a thick disk system, though it efficiently retains its angular momentum. Overall, the feedback in this case appears to be too strong, not only suppressing early, but also current

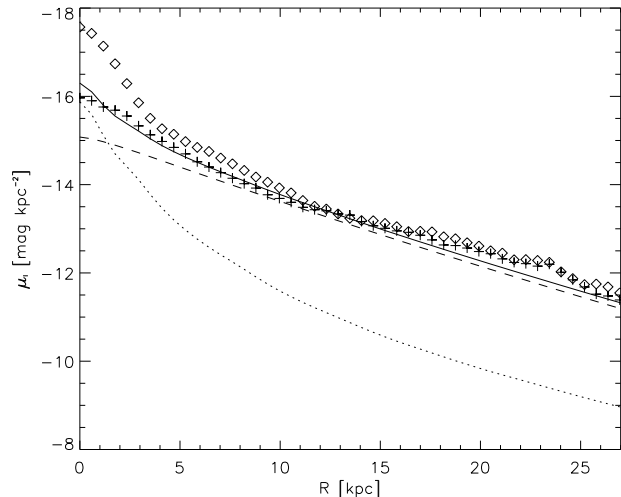


Figure 16. The effect of including kinetic feedback on the surface brightness profile for the face-on projection of the galaxy. The diamonds show the profile of the standard run, the crosses the run with kinetic feedback. The solid line is the final fit combining a bulge (dotted line) and a disk (dashed line) component.

star formation too much and therefore preventing the formation of a more dominant rotationally supported disk at $z=0$. This might be offset when including other effects like metal-dependent cooling. Also, a better tuning of the parameters in this model could improve the results, but that has to be left to future work.

Looking now at the differences the other, more conventional individual effects can cause, we first discuss the return of mass. As already expected, the differences here are small. The galaxy is systematically slightly brighter due to a slightly higher star formation rate which in turn is due to a higher cold gas fraction. The star formation history is more characterized by bursts, but generally the characteristics are comparable.

The model including type Ia supernovae is also similar. However, this is the only model efficiently reducing the dynamical bulge. The bulge-to-disk ratio B/D is 0.18 compared to 0.43 in the standard model. We attribute this mainly to a delayed peak in the star formation history, at $z \sim 2.15$ instead of $z \sim 2.6$. The height of the peak is not really reduced, but overall we have more gas and more younger stars which consequently have formed already in the disk progenitor and therefore are rotationally supported. They are not young enough to effectively brighten the galaxy though, and photometrically the bulge is more prominent. As already mentioned above, in the model combining type Ia supernovae and mass return we also implemented some basic metal tracking. The result is shown in Figure 15 for oxygen and iron abundances in the stars. In comparison to the observations of Milky Way stars by Bensby et al. (2004), the agreement with thick disk stars (green points) is reasonable, particularly in reproducing the trend (albeit with a large scatter). Compared to the thin disk stars (red points) our results are a little underabundant in iron. Since the model is rather crude this agreement is satisfactory and also in overall agreement with results by Scannapieco et al. (2005). Metal

enrichment is necessary for including metal-dependent cooling which will be discussed below.

The UV background shows influence on the star formation history only at lower redshift. The rather broad star formation peak of the standard model is sharply decreased at $z \approx 2$. In agreement with results by Navarro & Steinmetz (1997) less gas cools into the disk which is now surrounded by a halo of hot gas. The cold gas fraction is half of that in the standard model. The disk is slightly smaller but also brighter and more defined due to increased star formation particularly in the outer parts. The disk has slightly less angular momentum than in the standard case, and it is dynamically thicker at the expense of the thin rotationally supported component. This again follows the trend discussed by Navarro & Steinmetz (1997), who concluded that a UV background makes it even more difficult to form a high angular momentum disk since it predominantly reduces the accretion of late infalling high angular momentum gas. However, we find that including feedback can largely offset this negative effect, resulting in a slightly, but not dramatically smaller angular momentum.

More interesting than the UV background is the model with kinetic feedback since it is the only one of our physical models (except the blastwave model) with an almost pure exponential surface brightness profile for the face-on projection as shown in Figure 16. The outer parts of the profile are very similar to the standard run, but the bulge component in the inner 5 kpc is strongly reduced. The star formation history is characterized by a deep drop at $z \sim 2$, right after the first peak. The feedback generated from the first stars is able to heat and blow out gas, permanently reducing the baryon fraction within the virial radius to 0.11 (compared to a cosmic baryon fraction of 0.167). Later, gas is not blown out of the halo anymore, but its accretion onto the disk and therefore star formation in the disk is delayed, resulting in a brighter disk and a reduced mass-to-light ratio from 2.18 to 1.93, using the Chabrier IMF. The reduced star formation particularly at early times leads to a reduction in the galaxy mass by 30%, which is mostly a bulge reduction. The reduced bulge also leads to an increase in overall momentum making this our only run (besides the blastwave model and the high resolution run) with no angular momentum deficiency at all. The dynamical decomposition still shows a slightly reduced rotationally supported component and an increase in the thick disk.

Finally, including metal-dependent cooling basically offsets the feedback effects completely. Star formation happens efficiently at all times, especially very early resulting in a large peak of $\approx 60 M_{\odot} \text{ yr}^{-1}$ at $z \approx 3$. The feedback model is not able to regulate this at all. Star formation is still happening efficiently at $z=1$ and a thin young disk is present, but overall the system is strongly bulge dominated. Other effects are much needed to control particularly the early star formation.

7 COMBINING THE PHYSICAL MODELS

After studying each physical effect by itself, we now perform a series of runs with what we call the "all in" model, a combination of the UV background, kinetic feedback, type Ia supernovae and mass return. Acting in combination, they

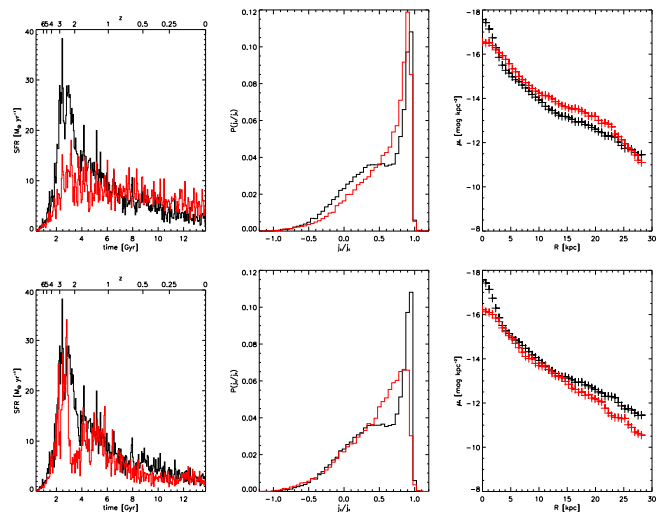


Figure 17. A comparison of our standard model (black) with the "all in" model (red) in terms of star formation history (left column), dynamical rotational support (middle column) and I-band surface brightness profile (right column). The bottom row shows the same comparison, but now with the "all in" model including metal-dependent cooling ("allmc").

of course will influence each other, which makes these runs more realistic than the individual cases we discussed before. We first discuss the result for the standard halo with standard resolution. Visually (see Figure 13), the resulting galaxy is one of the youngest with a strongly reduced bulge component. This is due to a very efficient suppression of early star formation leaving more gas for later accretion and leading to the highest current star formation rate of all our models, $5.7 M_{\odot} \text{ yr}^{-1}$. This suppression is a new effect due to the combination of all the models, since, though all suppress star formation a little at different times, none individually has such a large effect. This is shown in Figure 17 in the left panel of the top row. The middle panel shows the distribution of j_z/j_c as a measure of rotational support. Clearly the effect of the type Ia supernovae can be seen, shifting the emphasis from a bulge to a thick disk and also slightly increasing the peak of the thin disk with $j_z/j_c > 0.85$. This thickening of the disk can also be seen from the mock observational image of the edge on projection. Due to the quasi elimination of the early star formation peak, 80% of all stars in the final galaxy are now formed within the disk progenitor and therefore do not form a spheroidal configuration. But particularly the stars older than about 7 Gyr do not really remain in a tight thin disk, but their distribution thickens, leading to the final result.

In the right panel of Figure 17, we plot the surface brightness profile for the face-on projection of the disk and again we can identify the features contributed by the individual physical effects. The UV background is responsible for the increased level outside of a radius of about 18 kpc, with the sharp decline at the edge of the disk at ≈ 23 kpc. The kinetic feedback reduces the bulge brightness in the inner region. This is not as strong here as in Figure 16, which shows the model with kinetic feedback as the only effect, since the combination of type Ia supernovae, mass return

and UV background together result in some overall brightening of the whole galaxy. Overall, the galaxy characteristics are more realistic than before. Each effect plays some role in this, though the kinetic feedback seems to be the most important.

7.1 Including metal-dependent cooling

We now look at the "all in" run with metal dependent cooling included. Results in comparison to the standard model are shown in the bottom row of Figure 17. As we have already seen before in the run with standard feedback and metal-dependent cooling as an individual effect, the early star formation peak is strongly increased again. Since metal enrichment proceeds quickly in the areas where star formation can happen, the stronger cooling of gas with higher iron abundance can take over quickly as well, making gas cool more efficiently, form stars quicker and in turn speed up the enrichment. However, contrary to before, now the combined physical effects can regulate the increased star formation. The peak is narrow with a sharp drop (bottom left plot of Figure 17). The high early star formation also leads to an increased fraction of stars formed in clumps again, now 37% compared to 20% without metal dependent cooling. In combination with a lower star formation rate in the last 4 Gyr, this results in the strong reduction of the thin disk peak in the dynamical decomposition shown in the lower middle plot of Figure 17. The thin disk is rather unimportant dynamically with a mass fraction of only 17% and it is more a thick disk-bulge system. Photometrically, we have a fairly exponential profile with the kinetic effect of reducing the bulge acting in combination with a reduction of brightness in the outer regions of the disk. The UV background effects evidently have been canceled out by the stronger cooling. From this we can conclude that including other relevant physical effects, particularly kinetic feedback, helps to overcome the additional problems of increased star formation due to metal dependent cooling. However, a first high peak of star formation cannot be prevented, and as a result it is much more difficult to produce a dominant thin, rotationally supported disk at $z=0$.

7.2 The "all in" model in high resolution

The "all in" model is not fully converged when applied to our higher resolution halos. This can largely be attributed to the inclusion of kinetic feedback which has a rather strong impact on the surrounding region of the stellar particle. In the same way as in Figure 17 Figure 18 shows the effect of two variations of the "all in" model for the standard high resolution halo, MW_hr. In the bottom row of plots, the model is exactly the same as described in the previous section. The suppression of star formation is extremely efficient, creating a system with a rather low mass of $3.3 \times 10^{10} M_{\odot}$, only 40% of the stellar mass of the standard model and 60% of its luminosity. No thin disk is formed since there is only little star formation after $z \approx 1.5$. The galaxy has a rather low rotational velocity and is quite thick. However, in agreement with the impact of kinetic feedback in the standard resolution run, the bulge component in the photometric decomposition is reduced compared to the standard run. In order to

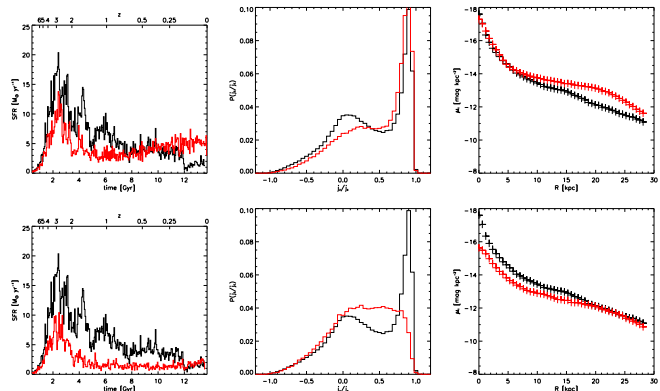


Figure 18. Comparison of the standard (black lines) model with the "all in" model (red lines) with 3% (top panel) and 10% (bottom panel) kinetic feedback for the standard halo in high resolution.

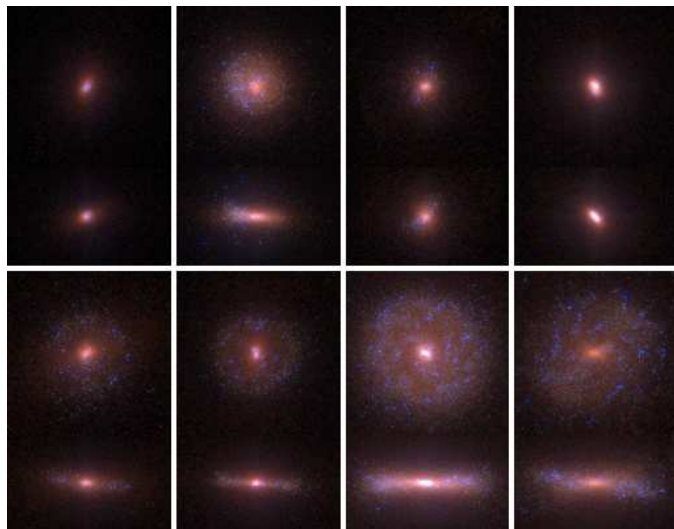


Figure 19. Mock observations of the halos with different masses run with the "all in" model and 3% kinetic feedback. The order is the same as in Figure 9 except for the plot in the lower right panel which shows the standard halo with 10% kinetic feedback in the "all in" model.

reduce the overly strong suppression of star formation and facilitate the formation of a young thin disk, we reduced the amount of kinetic feedback from 10% to 3%. As can be seen in the upper row of Figure 18, this is quite successful for the dynamical decomposition. We find a bulge-to-disk ratio of 0.57 while it is around 1 in the standard run and 1.26 in the original "all in" model. However, 3% is too little to drive out substantial material from the central region of the galaxy and the flattening of the surface brightness profile we saw in the standard resolution run with 10% kinetic feedback disappears completely. The disk still is substantially brightened in the outer parts leading to a lower mass-to-light ratio (1.7 compared to 2.06) and a more prominent thin disk than in the standard run. The galaxy has no angular momentum deficiency and, due to the higher luminosity at comparable rotational velocity, the agreement with the Tully-Fisher

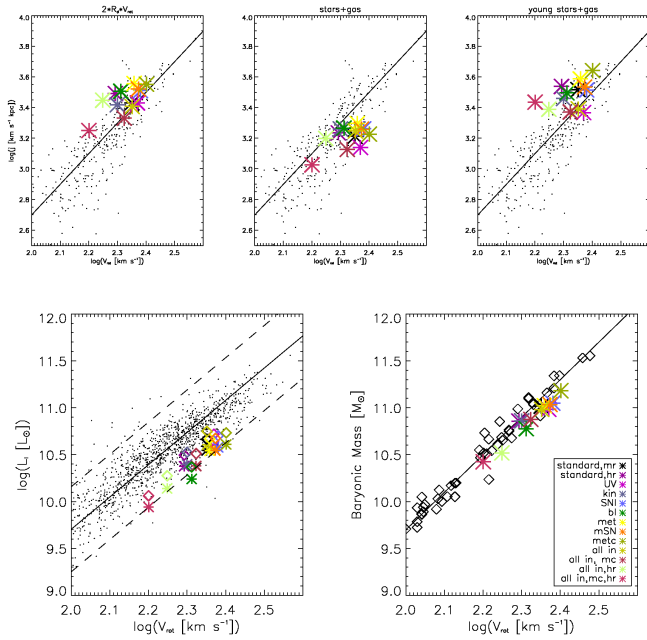


Figure 20. Scaling relations for the different physical models as shown in Table 4.

relation is improved (though still not perfect). Since this seems quite promising, we apply the low kinetic energy ”all in” model to all other halos with smaller masses than the standard run. The resulting mock observations are shown in Figure 19. Generally, for the lower mass halos the model is not very successful, with the exception of halo DM_hr2. All the others are rather spheroidal with low angular momentum and higher mass-to-light ratios than before in the standard model. This shows that the ”all in” model even with lower kinetic energy is quite dependent on the halo characteristics and also somewhat on resolution, and more work is needed to investigate particularly the behavior of the kinetic feedback.

8 THE INFLUENCE OF THE ADDITIONAL PHYSICS ON THE SCALING RELATIONS

Figure 20 shows the different physical models overplotted on the observational scaling relations. Since these runs have all been done with our standard halo, they scatter closely around the same value of rotational velocity of around 200 km s^{-1} . Most runs (with the exception of the model with kinetic feedback, the blastwave model and the high resolution model) are slightly angular momentum deficient. This is mainly due to the old stars in a more spheroidal configuration. In all cases there is a young stellar disk which, in combination with the cold gas disk, fits well on the angular momentum-size relation. This indicates again the difficulty of comparing the actual angular momentum to the exponential disk estimator. We conclude that the additional physical effects generally only mildly affect the angular momentum content, except for kinetic feedback, which retains it much better than the others. However, as we have shown in our angular momentum study in Paper 1, feedback itself is a

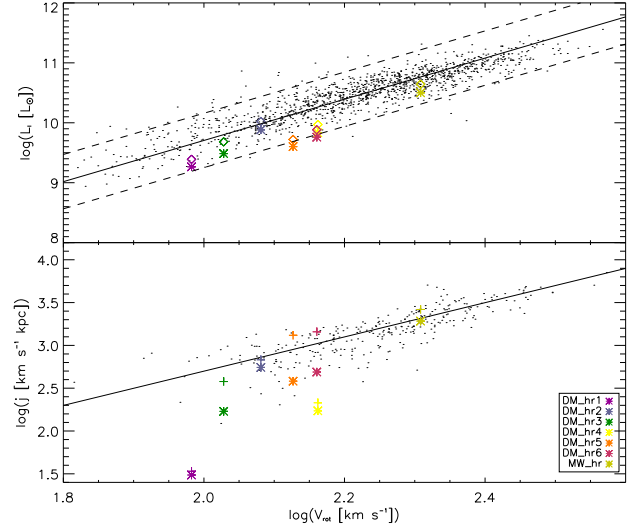


Figure 21. Tully-Fisher and angular momentum relation for the different mass halos with the ”all in” model with low kinetic feedback. In the upper panel, the star symbols are for a Salpeter IMF and the diamonds for a Chabrier IMF. The star symbols in the lower panel are the total angular momentum for the galaxy, the crosses for the disk of cold gas and young stars.

necessary ingredient to overcome the angular momentum problem.

For the Tully-Fisher (TF) relation, we find a spread along the relation, but no single physical effect can be tied to a strongly improved agreement with the observed relation. This is consistent with the generally similar mass-to-light ratios, which in all our models are between 2.5 and 3 for a Salpeter IMF and around 2 for a Chabrier IMF. While the agreement is good with the baryonic TF relation independent on the physical model used, there is some variation among the models with respect to the photometric TF relation. The lower the mass-to-light ratio, the better the agreement with the TF relation. The standard resolution ”all in” model as well as the high resolution ”all in” model with low kinetic feedback both agree best. With $M/L=1.7$ the latter has the lowest overall mass-to-light ratio. This leads us to the conclusion, that in general one physical effect might induce small changes to the galaxy, but a big impact can only be achieved with a combination. Our ”all in” model, with its flaws, seems to be promising in this respect.

The results of applying the ”all in” model with low kinetic energy to the lower mass halos is also in agreement with the conclusion drawn above. Their fit to the scaling relations are shown in Figure 21. This plot indicates a connection between angular momentum deficiency and poor agreement with the photometric TF relation. The halos disagreeing with both relations also tend to have high mass-to-light ratios. Only in two halos, the standard halo and DM_hr2, does the ”all in” model result in an improved (in the latter case actually excellent) agreement with all scaling relations. Both halos are the only ones close to the observed Tully Fisher-relation (top panel of Figure 21). They are also the only halos with no angular momentum deficiency at all (already in the standard model and also in the ”all in” model;

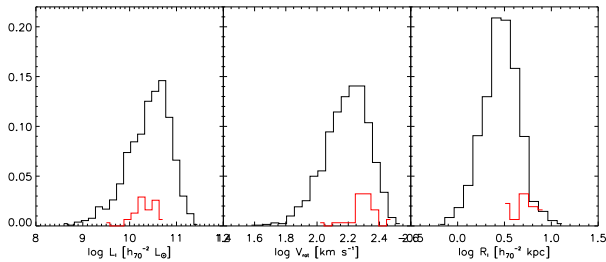


Figure 22. The distribution of our galaxies (red curves) compared with observed data (black curves) from Courteau et al. (2007), both normalized by their respective number of objects.

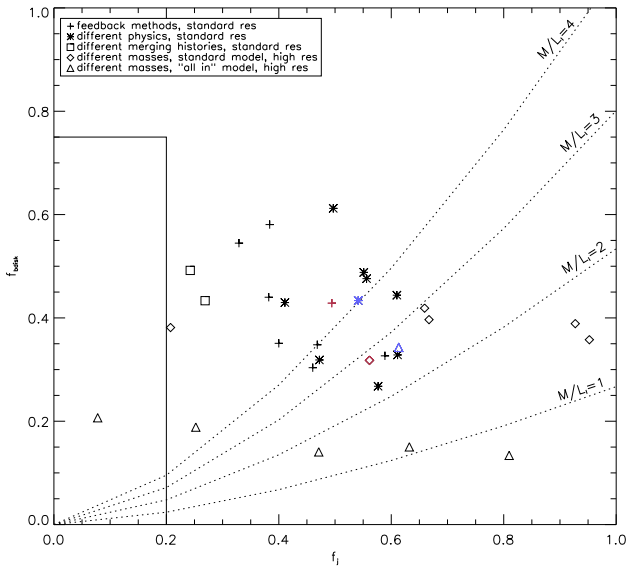


Figure 23. Fraction of baryons assembled into the galaxy ($f_{b,disk}$) vs. the ratio between the specific angular momentum of the disk and its surrounding halo (f_j). The square marked by solid lines denotes the region populated by early simulated galaxies (Navarro & Steinmetz 2000b). The red colored symbols show the standard halo with the standard model in standard (cross) and high (diamond) resolution. The blue colored symbols show the standard halo with the "all in" model for standard (star) and high (triangle) resolution.

bottom panel of Figure 21). They have in common the quietest merging histories of all our halos. They also have rather stable star formation histories (halo DM_hr2 basically lacks an early star formation peak). If this is the prerequisite to form a reasonable disk galaxy, then again the question is raised how the number of disk galaxies in the present day universe can be reconciled with the high numbers of large mergers in a Λ CDM universe.

9 DISCUSSION AND CONCLUSIONS

We have performed a detailed study of supernova feedback mechanisms in a Milky Way-type halo, but also in a range

of other halos spanning different masses and different merging histories, using a medium and a high resolution. Out of a variety of methods of distributing feedback energy we picked the one with the best performance to be our standard model. The important feature for the suppression of the formation of a large bulge was mainly to turn off cooling locally to mimic a multiphase medium. The difference in the results between the distribution methods themselves is comparatively small. The standard model is a model with an energy output following an exponential law, local cooling turnoff and a variable smoothing length for the supernova energy. It was then applied to halos with different masses and merging histories and improved with additional relevant physical effects. The first question one might ask is how typical are our resulting galaxies. In Figure 22, we compare them to observed data (from Courteau et al. 2007) with respect to the most interesting parameters of disk galaxies: the I band luminosity, the rotational velocity and the I band disk scale length. Our galaxies are typical in terms of their luminosity. The low outlier is our lowest mass halo. Their rotational velocities are slightly high, but well within the distribution. The disk scale lengths are all somewhat high. Even though we attempted to measure them in the same way as an observer would, this is not straightforward and there may be systematic effects, especially due to the rotation curves. While our rotation curves for the standard halo are mostly flat enough that the exact measuring point does not matter, this is not always the case for the lower mass halos, especially in the "all in" model.

From our study of different physical properties we can conclude that a combination of type Ia supernovae, some fraction of kinetic feedback and a UV background improves the result significantly towards a more realistic disk. Particularly interesting is the kinetic feedback, which efficiently blows out gas from the progenitor and reduces the importance of the central bulge making the disk more exponential. However, this is a very harsh way of changing the gas conditions and difficult to simply extend to higher resolution. In our high resolution runs, we had to reduce the kinetic energy fraction from 10% to 3% to achieve reasonable results, despite the resulting loss of the flattening effect in the surface brightness profile. Further investigation seems necessary here to improve the stability of the model.

We also find that it is not enough to simply reduce the early peak in star formation. This reduction leaves a lot of gas for later accretion and star formation. It reduces the photometric importance of the bulge, but also tends to thicken the disk. Dynamically, the only way to decrease the bulge-to-disk ratio seems to be a delay of the star formation peak, as in our case with the effect of type Ia supernovae, or to prevent the gas to enter the disk at a later point in time.

Including metal dependent cooling has a significant impact and actually raises the early star formation peak again, making it more difficult to form a disk. In combination with the other effects, this can be controlled, but the result is not quite satisfactory yet, indicating that a more complex model might be necessary. However, our metal enrichment is very basic. It seems to be in general agreement with other simulations and also with observations, but more extensive testing would be necessary to study enrichment processes. Still, we believe that including metal dependent cooling is important to correctly evaluate the performance of the feedback model.

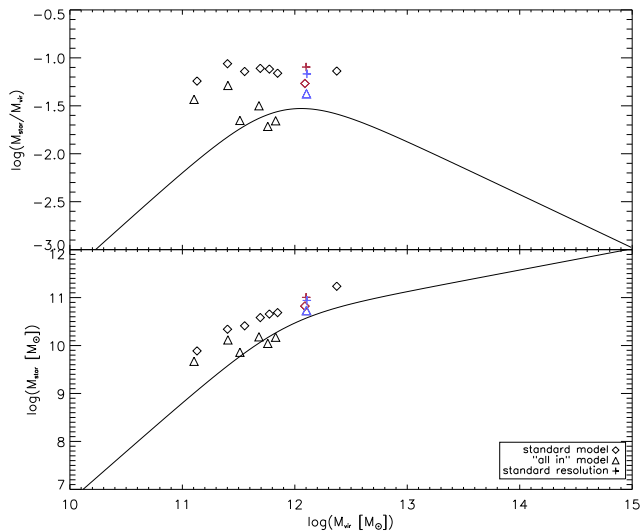


Figure 24. The stellar-to-halo mass relation by Moster et al. (2009) in comparison with our simulated high resolution halos of different masses. The red and blue symbols indicate the standard, Milky Way mass halo, while the crosses are the same halo in standard resolution.

We also briefly looked at a blastwave-type feedback. Our model is not as sophisticated as in Stinson et al. (2006), since for example we did not include feedback energy output depending on the lifetime of the stars. In our case this feedback is extremely strong and reduces overall star formation too much to create a Milky Way-type galaxy. However, a fine-tuning of parameters could lead to improvements and other effects might also balance this. It would be particularly interesting to look at metal-dependent cooling in this respect since stronger cooling at early times needs stronger feedback to maintain a low star formation rate.

Our galaxies all fit well on the angular momentum-size relation, so they do not suffer from the earlier problem of too compact, centrally concentrated disks. This is primarily a result of the feedback, not an effect of a high resolution (see Paper 1). The actual angular momentum content of gas and stars in our simulated galaxies is mostly within the scatter of observed galaxies (with the exception of some of our halos where no real disk was formed at all), but on the lower end with about 60-80% of the expected relation. The only runs with no angular momentum deficiency are those with kinetic feedback and with the blastwave model. This is alleviated when looking only at the angular momentum of the actual disk consisting of young stars and cold gas. For the total angular momentum of the galaxy we find a systematic offset when comparing directly to the angular momentum calculated, as observers do, from $j = 2R_d V_{\text{rot}}$, which disappears when looking only at the angular momentum of the disk made of young stars and cold gas. A comparison between observations and simulations is therefore only meaningful for clearly disk-dominated galaxies.

9.1 The Tully-Fisher relation as a benchmark test

The biggest challenge for a successful disk galaxy simulation remains to fit the Tully-Fisher relation. We manage to fit the baryonic Tully-Fisher relation quite well, as well as the slope for the photometric relation, but we fail to reproduce the zero-point. From this we conclude that the structure of our simulated galaxies is realistic. Including different physical effects scatters the galaxies along the photometric relation rather than improving the fit. The "all in" model, with a combination of several effects, does result in an improvement over the standard model. For a Salpeter IMF we improve from an offset factor of ≈ 2.4 to 1.9, and for a Chabrier IMF from ≈ 1.8 to 1.4. However, the agreement is still not satisfying. It is difficult to separate out the underlying reason for the problem. It can either be that the luminosity is too low, or that the rotational velocity is too high, or a combination of both. One hint might come from the stellar mass-to-light ratios which in our case are about 2 (based on a Chabrier IMF) with the "all in" runs of the standard halo being improved to ≈ 1.6 both in standard and in high resolution. These increases again to about 2 when metal-dependent cooling is included. Further information comes from Figure 23 where we follow Navarro & Steinmetz (2000b) in plotting the fraction of baryons assembled into the galaxy vs. the ratio between the specific angular momentum of the disk and its surrounding dark matter halo. The simulated galaxies by Navarro & Steinmetz (2000b) were all placed within the squared region indicated by the solid lines. While a large fraction of the baryons were assembled into galaxies, they had only very little angular momentum. Our galaxies with their much higher angular momentum content are much more distributed over the whole range of the plot, but, with respect to the baryonic content, lie still preferably in the upper region, above a fraction of 30% of baryons being assembled into the disk. Exceptions are the lower mass halos with the "all in" model. Since typical disk galaxies have a mass-to-light ratio of around 1-1.5, our galaxies clearly contain too much mass or are too dim for the stellar mass they have. From semi-analytical models we know that small baryon fractions are needed to reach an agreement between the stellar mass function and the halo mass function. In comparison with this our baryonic mass in the disk is too large. This is confirmed by a comparison with the results by Moster et al. (2009), who derived a stellar-to-halo mass (SHM) relation determined by the constraint to fit the observed SDSS stellar mass function and correlation functions. This SHM relation is shown in Figure 24, together with the results for our high resolution simulations of different mass halos. The simulations with the standard model are shown with diamonds and the ones with the "all in" model with triangles. The Milky Way halo results are the red and blue symbols, respectively, while the crosses show the corresponding result for the standard resolution halo. Our model produces a systematic offset towards higher stellar masses which is worse for the lowest mass halos. While the "all in" model is able to improve on that, we know from above that these stars form a little bit too early and therefore are too dim to fit the Tully-Fisher relation. As a side note it should be mentioned that this curve does depend on the observed mass of the Milky Way dark matter halo which is still under

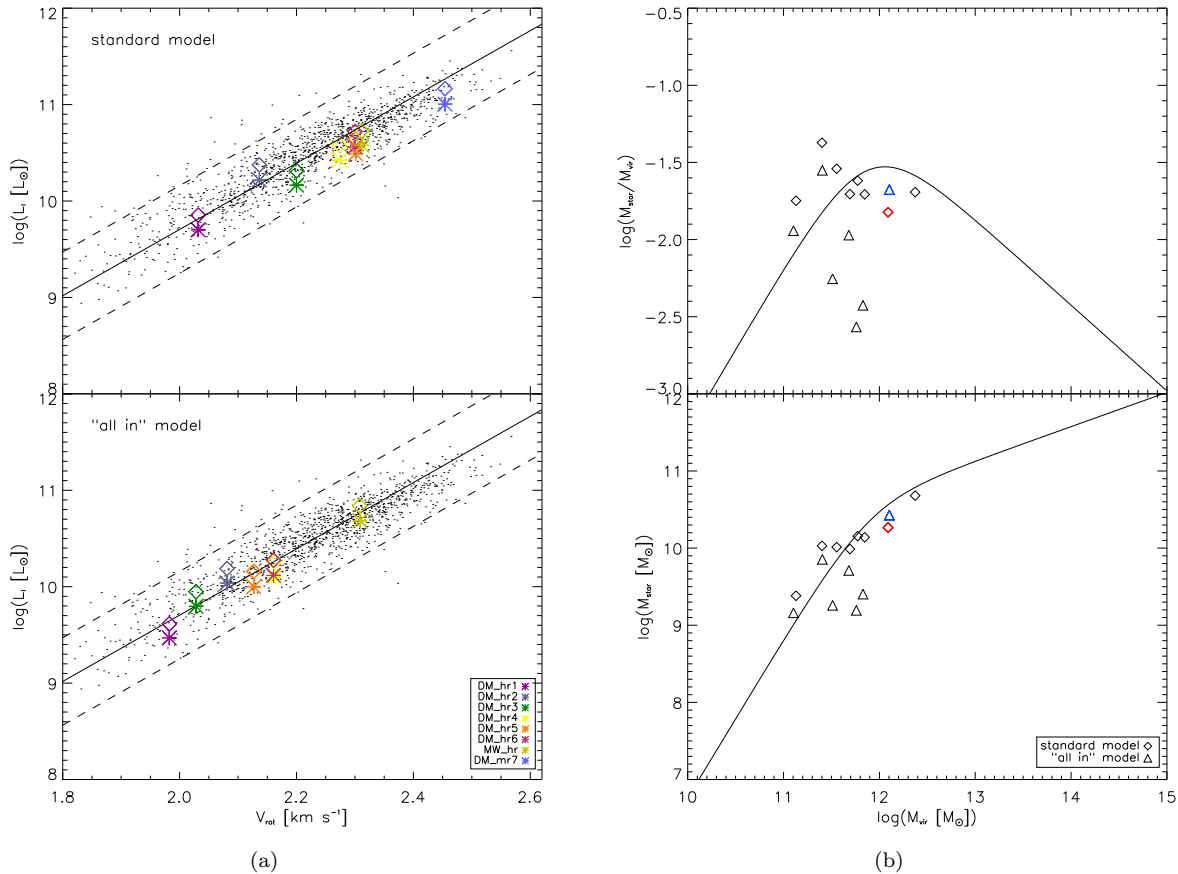


Figure 25. Panel (a): Tully-Fisher relation with luminosities computed assuming that the bulges have the same mass-to-light ratio as the disk. Panel (b): Same as Figure 24, but with stellar masses excluding the bulge stars.

discussion. Recent results from SDSS and the RAVE survey³ point to a smaller mass (Smith et al. 2007) which would decrease the gap between the curve and our simulated data (Xue et al. 2008).

In Figure 25, using ad-hoc assumptions, we explore ways on how to improve the agreement with the Tully-Fisher relation and the SHM relation. Looking only at our disks made up of mostly young stars, they have mass-to-light ratios of around 1.5 for a Salpeter and even 1 to 1.3 for a Chabrier IMF, which is in the range of observed disk galaxies. For the different mass halos we therefore compute new total luminosities assuming bulge luminosities based on the same mass-to-light ratio as the disks. This is an attempt to model what the galaxies would look like if the early star formation peak would be delayed by some mechanism, possibly stronger stellar feedback. (We have a small delay for the model including type Ia supernova feedback, which does reduce the bulge, but the effect is not big enough.) This results in an excellent fit of the Tully-Fisher relation as shown in Figure 25(a) for the standard model (top panel) and the "all in" model (bottom panel). Since with this method only the luminosity is adjusted, but the total stellar mass is not re-

duced, it would not result in an improved agreement with the SHM relation. If a mechanism could be devised which not only would delay the early star formation, but also prevent this gas from ever forming stars, and therefore a bulge, for example by blowing it out efficiently or keeping it hot, the mass would be reduced. Figure 25(b) shows that in this case, when only the stellar mass of the disk is taken into account, a good agreement with the SHM relation is achieved for the standard model, though the shape cannot be reproduced well. In the "all in" model, where the masses are lower, the disk alone is not massive enough to fit the relation. An attempt to reproduce the Tully-Fisher relation under the same assumption of taking out the bulge stars completely was not successful. The effect of a smaller rotational velocity due to the reduced mass is erased by the considerably reduced luminosity. This could be because the disk mass-to-light ratios are smaller, but not small enough. However, for the Chabrier IMF, they are close to 1 at least for some of the galaxies. Another possible explanation is too much dark matter in the halo dominating the rotation curve and maintaining a high rotational velocity. This high dark matter concentration could also be a partial explanation of the slightly low baryon fraction we find in some of our halos.

³ The **R**adial **V**elocity **E**xperiment is measures radial velocities, metallicities and abundance ratios for up to a million stars in the Milky Way. See www.rave-survey.aip.de for more information.

We conclude that even our more complex and realistic "all in" model is not in complete agreement with the Tully-Fisher relation, though the galaxies are within the observed

scatter. An exception is halo DM_hr2. Improvements could be made in the implementation of already included effects (like a blastwave approach) or with the addition of new effects, for example an efficient wind model. However, from the discussion above, it seems that an improved fit to both the Tully-Fisher and the SHM relation is possible only when the formation of the bulge is largely prevented and the gas is kept outside the galaxy permanently. None of the physical effects we tested was efficient enough to be responsible for this. Our results indicate a possible further complication in the high concentration of the dark matter halo, which could be a basic problem of Λ CDM. We obtain the best results with two halos with the most quiet merging histories, in line with the typical assumptions for disk galaxies but in tension with Λ CDM's hierarchical structure.

In summary we find the question of the formation of realistic disk galaxies in cosmological simulations a highly interconnected, complex problem that is difficult to handle in a controlled manner. Particularly the complex feedback models require a recalibration when increasing the resolution. The answer to the pending problem of forming realistic disks does not seem to be a single physical or numerical effect, but rather a combination of many little effects whose interplay has to be scrutinized carefully and systematically to find the solution.

ACKNOWLEDGEMENTS

We thank Stefan Gottlöber and Gustavo Yepes for providing initial conditions and Volker Springel for providing a version of GADGET2 which included radiative cooling. This work was funded through a grant by the German Research Foundation (DFG) under STE 710/4 as part of the Priority Programme SPP1177 "Witnesses of Cosmic History: Formation and evolution of black holes, galaxies and their environment".

REFERENCES

- Abadi, M.G., Navarro, J.F., Steinmetz, M., Eke, V.R., 2003, *ApJ*, 591, 499
- Abadi, M.G., Navarro, J.F., Steinmetz, M., Eke, V.R., 2003, *ApJ*, 597, 21
- Bensby, T., Feltzing, S., Lundström, L., 2004, *A&A*, 415, 155
- Blumenthal, G.R., Faber, S.M., Primack, J.R., Rees, M.J., 1984, *Nature*, 311, 517
- Bruzual, G., Charlot, S., 2003, *MNRAS*, 344, 1000
- Bullock, J.S., Stewart, K.R., Purcell, C.W., 2009, in Andersen J., Bland-Hawthorn J., Nordström B., eds, *IAU Proc. Symp. 254, The Galaxy Disk in Cosmological Context*. Cambridge Univ. Press, Cambridge, p.85
- Cappellaro, E., Evans, R., Turatto, M., 1999, *A&A*, 351, 459
- Ceverino, D., Klypin, A., 2009, *ApJ*, 695, 292
- Chabrier, G., 2003, *PASP*, 115, 763
- Chevalier, R.A., 1974, *ApJ*, 188, 501
- Cole, S., Helly, J., Frenck, C.S., Parkinson, H., 2008, *MNRAS*, 383, 546
- Courteau, S., Dutton, A.A., van den Bosch, F.C., MacArthur, L.A., Dekel, A., McIntosh, D.H., Dale, D.A., 2007, *ApJ*, 671, 203
- Davé, R., Hernquist, L., Katz, N., Weinberg, D.H., 1999, *ApJ*, 511, 521
- Davis, M., Efstathiou, G., Frenck, C.S., White, S.D.M., 1985, *ApJ*, 292, 371
- de Blok, W.J.G., Walter, F., Brinks, E., Trachternach, C., Oh, S.-H., Kennicutt, R.C., 2008, *AJ*, 136, 2648
- Fall, S.M., Efstathiou, G., 1980, *MNRAS*, 193, 189
- Gerritsen, J.P.E., 1997, PhD.thesis, Kapteyn Astron.Inst., The Netherlands
- Gingold, R.A., Monaghan, J.J., 1977, *MNRAS*, 181, 375
- Giovanelli, R., Haynes, M.P., Herter, T., Vogt, N.P., Wegner, G., Salzer, J.J., da Costa, L.N., Freudling, W., 1997, *AJ*, 113, 22
- Gottlöber, S., Klypin, A., Kravtsov, A.V., 2001, *ApJ*, 546, 223
- Governato, F., Mayer, L., Wadsley, J., Gardner, J.P., Willman, B., Hayashi, E., Quinn, T., Stadel, J., Lake, G., 2004, *ApJ*, 607, 688
- Governato, F., Willman, B., Mayer, L., Brooks, A., Stinson, G., Valenzuela, O., Wadsley, J., Quinn, T., 2007, *MNRAS*, 374, 1479
- Governato, F., Brook, C.B., Brooks, A.M., Mayer, L., Willmann, B., Jonsson, P., Stilp, A.M., Pope, L., Christensen, C., Wadsley, J., Quinn, T., 2008, arXiv:0812.0379 [astro-ph]
- Haardt, F., Madau, P., 1996, *ApJ*, 461, 20
- Katz, N., 1992, *ApJ*, 391, 502
- Katz, N., Weinberg, D.H., Hernquist, L., 1996, *ApJS*, 105, 19
- Kautsch, S.J., Grebel, E.K., Barazza, F.D., Gallagher, J.S.III, 2006, *A&A*, 445, 765
- Kawata, D., Gibson, B.K., 2005, *MNRAS*, 358, 16
- Kennicutt, R.C., 1998, *ApJ*, 498, 541
- Khalatyan, A., Cattaneo, A., Schramm, M., Gottlöber, S., Steinmetz, M., Wisotzki, L., 2008, *MNRAS*, 387, 13
- Lucy, L.B., 1977, *ApJ*, 82, 1013
- McGaugh, S., 2005, *ApJ*, 632, 859
- McKee, C.F., Ostriker, J.P., 1977, *ApJ*, 218, 148
- Miller, G.E., Scalo, J.M., 1979, *ApJS*, 41, 51
- Mo, H.J., Mao, S., White, S.D.M., 1998, *MNRAS*, 295, 319
- Moster, B.P., Somerville, R.S., Maulbetsch, C., van den Bosch, F.C., Macciò, A.V., Naab, T., Oser, L., 2009, arXiv:0903.4682 [astro-ph.CO]
- Navarro, J.F., White, S.D.M., 1993, *MNRAS*, 265, 271
- Navarro, J.F., White, S.D.M., 1994, *MNRAS*, 267, 401
- Navarro, J.F., Steinmetz, M., 1997, *ApJ*, 478, 13
- Navarro, J.F., Steinmetz, M., 2000, *ApJ*, 528, 607
- Navarro, J.F., Steinmetz, M., 2000, *ApJ*, 538, 477
- Okamoto, T., Eke, V.R., Frenk, C.S., Jenkins, A., 2005, *MNRAS*, 363, 1299
- Park, C., Choi, Y.-Y., Vogeley, M.S., Gott, J.R.I., Blanton, M.R. 2007, *ApJ*, 658, 898
- Peebles, P.J.E., 1982, *ApJ*, 263, L1
- Peng, C.Y., Ho, L.C., Impey, C.D., Rix, H.-W., 2002, *AJ*, 124, 266
- Piontek, F., Steinmetz, M., 2009, submitted to *MNRAS*
- Raiteri, C.M., Villata, M., Navarro, J.F., 1996, *A&A*, 315, 105
- Robertson, B., Yoshida, N., Springel, V., Hernquist, L.,

- 2004, ApJ, 606, 32
- Robertson, B., Bullock, J.S., Cox, T.J., Di Matteo, T., Hernquist, L., Springel, V., Yoshida, N., 2006, ApJ, 645, 986
- Salpeter, E.E., 1955, ApJ, 121, 161
- Scannapieco, C., Tissera, P.B., White, S.D.M., Springel, V., 2005, MNRAS, 364, 552
- Scannapieco, C., Tissera, P.B., White, S.D.M., Springel, V., 2006, MNRAS, 371, 1125
- Scannapieco, C., Tissera, P.B., White, S.D.M., Springel, V., 2008, MNRAS, 389, 552
- Scannapieco, C., White, S.D.M., Springel, V., Tissera, P.B., 2008, MNRAS, 396, 696
- Schmidt, M., 1995, ApJ, 129, 243
- Schneider, P., 2006, Einführung in die extragalaktische Astronomie und Kosmologie, Berlin: Springer
- Smith, M.C., Ruchti, G.R., Helmi, A., Wyse, R.F.G., Fulbright, J.P., Freeman, K.C., Navarro, J.F., Seabroke, G.M., Steinmetz, M., Williams, M., Bienaymé, O., Binney, J., Bland-Hawthorn, J., Dehnen, W., Gibson, B.K., Gilmore, G., Grebel, E.K., Munari, U., Parker, Q.A., Scholz, R.-D., Siebert, A., Watson, F.G., Zwitter, T., 2007, MNRAS, 379, 755
- Spergel, D.N. et al., 2007, ApJS, 170, 377
- Springel, V., 2005, MNRAS, 364, 1105
- Springel, V., Hernquist, L., 2003, MNRAS, 339, 312
- Steinmetz, M., Müller, E., 1995, MNRAS, 276, 549
- Stinson, G., Seth, A., Katz, N., Wadsley, J., Governato, F., Quinn, T., 2006, MNRAS, 373, 1074
- Sutherland, R.S., Dopita, M.A., 1993, ApJS, 88, 253
- Thielemann, F.-K., Nomoto, K., Yokoi, K., 1986, A&A, 158, 17
- Wechsler, R.H., Bullock, J.S., Primack, J.R., Kravtsov, A.V., Dekel, A., 2002, ApJ, 568, 52
- Weinmann, S.M., van den Bosch, F.C., Yang, X., Mo, H.J. 2006, MNRAS, 366, 2
- Wetzel, A.R., Cohn, J.D., White, M., 2009, MNRAS, 395, 13766
- White, S.D.M., Frenk, C.S., 1991, ApJ, 379, 52
- White, S.D.M., Rees, M.J., 1978, MNRAS, 183, 341
- Wosley, S.E., Weaver, T.A., 1995, ApJS, 101, 181
- Xue, X.X., Rix, H.W., Zhao, G., Re Fiorentin, P., Naab, T., Steinmetz, M., van den Bosch, F.C., Beers, T.C., Lee, Y.S., Bell, E.F., Rockosi, C., Yanny, B., Newberg, H., Wilhelm, R., Kang, X., Smith, M.C., Schneider, D.P., 2008, ApJ, 684, 1143
- Yepes, G., Kates, R., Khokhlov, A., Klypin, A., 1997, MNRAS, 284, 235